Palaeogeography, Palaeoclimatology, Palaeoecology 548 (2020) 109630

Contents lists available at ScienceDirect

Palaeogeography, Palaeoclimatology, Palaeoecology

journal homepage: www.elsevier.com/locate/palaeo

Tuff fingerprinting and correlations between OGCP cores and outcrops for Pre-Bed I and Beds I/II at Olduvai Gorge, Tanzania

Lindsay J. McHenry[a,*], Ian G. Stanistreet[b,c], Harald Stollhofen[d], Jackson K. Njau[c,e], Nicholas Toth[c], Kathy Schick[c]

[a] Department of Geosciences, University of Wisconsin-Milwaukee, 3209 N. Maryland Ave., Milwaukee, WI 53211, USA
[b] Dept. Earth, Ocean and Ecological Sciences, University of Liverpool, Brownlow Street, Liverpool L69 3GP, UK
[c] The Stone Age Institute, Bloomington, IN 47407-5097, USA
[d] GeoZentrum Nordbayern, Friedrich-Alexander-University (FAU) Erlangen-Nürnberg, Schloßgarten 5, 91054 Erlangen, Germany
[e] Department of Earth and Atmospheric Sciences, Indiana University, 1001 East 10th Street, Bloomington, IN 47405-1405, USA

ARTICLE INFO

Editor: H Howard Falcon-Lang

Keywords:
Pleistocene
Tephrostratigraphy
Geochemistry
Mineral assemblage
East Africa
Tephra

ABSTRACT

Sediment cores retrieved from the Pleistocene Olduvai Basin by the Olduvai Gorge Coring Project (OGCP) provide a high resolution record of tuffs and other volcaniclastic deposits, together with a lacustrine sedimentary record full of paleoenvironmental indicators. Correlating tuffs between the cores and outcrops at Olduvai, where these tuffs are identified at paleoanthropologically important sites, is critical for applying the new paleoenvironmental data to the conditions under which hominins lived. Tuffs and other volcaniclastic deposits from three cores were analyzed for mineral assemblages and glass and mineral major element compositions (feldspar, augite, hornblende, titanomagnetite, and glass where possible) to compare to published geochemical fingerprint data, based on marker tuffs from outcrop equivalents at Olduvai Gorge. In combination with stratigraphic position, these mineralogical and geochemical data were used to correlate between the cores and outcrops, providing direct temporal tie-lines between the cores and sites of paleoanthropological interest. Direct correlations are most certain for Olduvai Bed I, where all major tuff markers from outcrop are identified for one or more of the three core sites, and for the upper part of the underlying Ngorongoro Formation, which includes the Coarse Feldspar Crystal Tuff (CFCT) and Naabi ignimbrites exposed in the oldest Pleistocene exposures of the Western Gorge. Also characterized were the mineral and glass compositions of tuffs and ignimbrites pre-dating the oldest exposed outcrop units, extending our record of explosive events from the Ngorongoro Volcano. While no specific correlations can be confirmed between individual Bed II tuffs in the cores and in outcrops, correlations are possible between the cores themselves (using newly identified tuff compositions), and some potential correlations (non-unique, based on individual mineral phases) between core and outcrop can be used in conjunction with other stratigraphic tools to help constrain the intervals in question.

1. Introduction

The palaeoanthropologically-important Pleistocene strata of Olduvai Gorge, Tanzania contain abundant pyroclastic material derived from the adjacent Ngorongoro Volcanic Highlands, preserved in primary and reworked tuffs and as a component of various other volcaniclastic deposits (e.g., diamictites, conglomerates, sandstones derived from volcanic materials). A tephrostratigraphic framework based on these volcanic units helps correlate between different sites within the Olduvai Basin. Recent cores recovered by the Olduvai Gorge Coring Project (OGCP) from the Olduvai paleolake depocenter (Fig. 1) contain many of the same units, hosting a high-resolution paleoclimatic record. This study aims to characterize the tuffs and volcaniclastic sandstones of the OGCP cores in terms of their stratigraphic position, mineral assemblages, and mineral and glass compositions, and compare these against the mineralogical and geochemical "fingerprints" previously established for the Olduvai tuffs in outcrop. This work is therefore essential to establish correlations between the cores and the Olduvai outcrop stratigraphy, thus relating the paleoclimatic record derived from the cores to the classic Olduvai hominin sites. These sites document changes in hominin species (*Homo habilis, Homo erectus, Paranthopus boisei,* and *Homo sapiens*) and stone tool technologies (Oldowan, Acheulean, and Middle Stone Age), together with a record of the paleoecological context (e.g. Leakey, 1951, 1965, 1966, 1971; Leakey

* Corresponding author.
E-mail address: lmchenry@uwm.edu (L.J. McHenry).

https://doi.org/10.1016/j.palaeo.2020.109630
Received 29 May 2019; Received in revised form 14 September 2019; Accepted 31 January 2020
Available online 13 February 2020
0031-0182/

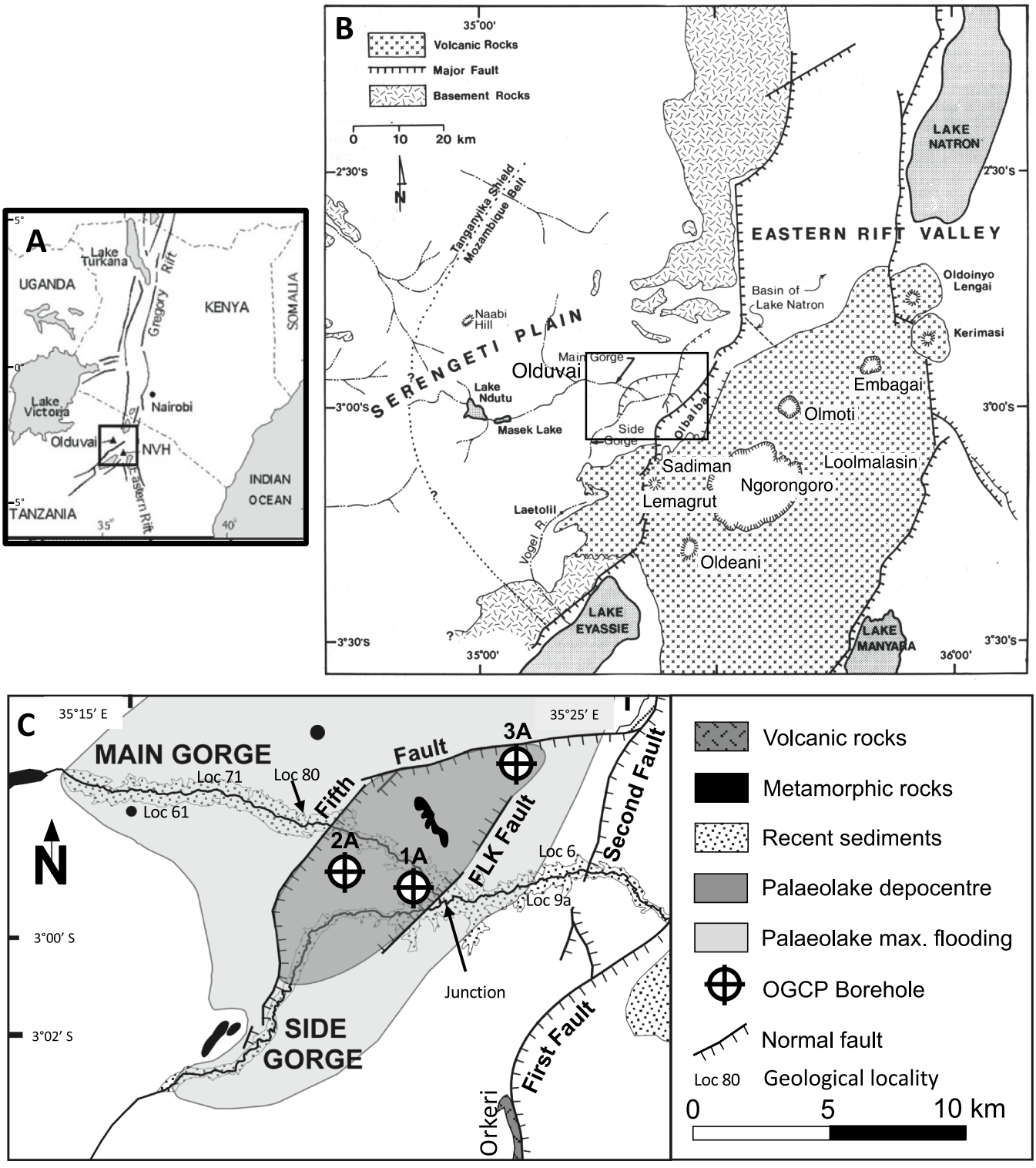

Fig. 1. Maps showing location of Olduvai Gorge, and of the locations of the borehole sites. A. Map of East Africa, showing location of Olduvai Gorge. B. Map of the Olduvai region, showing the location of source volcanoes in the adjacent Ngorongoro Volcanic Highlands. Modified after Ashley and Hay (2002). C. Map of Olduvai Gorge, with the positions of Cores 1A, 2A, and 3A/3B indicated, along with specific localities mentioned in the text. Geological locality numbers after Hay, 1976. In B and C, the white background represents areas with modern soil/grassland cover with limited exposure.

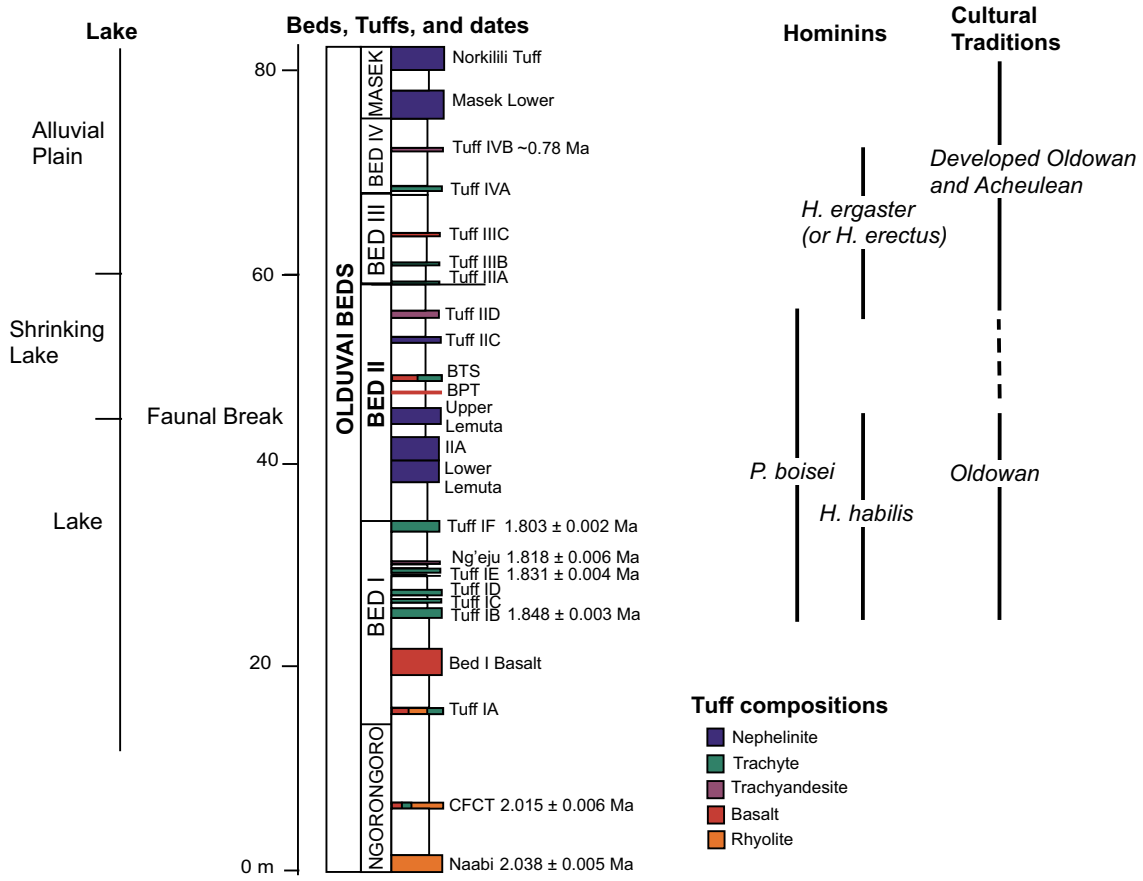

Fig. 2. Composite stratigraphic column for Olduvai based on outcrop exposures. Colors indicate general tuff composition (e.g. rhyolite vs. trachyte) and show a general change over time, from rhyolites near the base (Naabi Ignimbrite), trachytes in Upper Bed I, and nephelinite compositions in Bed II and higher. Dates for individual tuffs from Deino (2012). To the right are the overall hominin species and lithic technology trends observed in the Olduvai record, after Klein, 1999.

et al., 1964). This study also documents the changes in volcanic compositions over time, which tracks the evolution of the Ngorongoro Volcanic Highlands through the Pleistocene.

2. Background

Tuffaceous units are used at Olduvai as chronostratigraphic timeplanes throughout the Olduvai Basin, in some cases marking the boundaries between various Beds of the Olduvai Beds (e.g. Tuff IF at the boundary between Beds I and II). Such correlations have been based on physical mapping (e.g. Hay, 1976), and more recently based on mineral and glass compositional "fingerprints" (e.g. McHenry, 2005, 2012; McHenry et al., 2016; Habermann et al., 2016; McHenry and Stanistreet, 2018). Fig. 2 shows a composite stratigraphic section of the Olduvai Beds, focusing on the compositions of the associated tuff markers. The acquisition of high-quality cores from the Olduvai Formation in 2014 by the Olduvai Gorge Coring Project (OGCP) provides an opportunity to apply these fingerprints to a well-preserved, continuous tephrostratigraphic record from three sites within the basin. These established fingerprints also allow for direct correlation between the new cores (and their associated paleoenvironmental proxies) and outcrops, establishing the chronostratigraphic framework for the cores and linking them directly to the world-famous paleoanthropological record of Olduvai Gorge.

2.1. Introduction to the OGCP cores

Over the past decade, researchers with an interest in the paleoecology of hominin evolution have drilled and recovered cores from paleolakes in the East African Rift to acquire detailed lacustrine paleoenvironmental records to complement existing paleoanthropological records from outcrop studies. These studies include The Hominin Sites and Paleolakes Drilling Project (HSPDP), which recovered cores from paleolakes in North Awash and Chew Bahir (Ethiopia) and West Turkana, Baringo, and Lake Magadi (Kenya), and the Olorgesailie Drilling Project (Kenya) (Cohen et al., 2016; Campisano et al., 2017). The OGCP cores continue this record southwards into Tanzania. In July 2014, the OGCP recovered four cores from three sites at Olduvai, targeting previously reconstructed depocenters of the Olduvai paleolake during different intervals (Core 2A: Bed I, (S 2° 58′ 43.0″, E 35° 19′ 25.5″), Core 1A: Upper Bed II, (S 2° 59′ 8.2″, E 35° 20′ 34.1″), and Cores 3A and 3B: Bed III-younger (S 2° 56′ 41.6″, E 35° 22′ 51.5″), after Hay (1976), see core positions in Fig. 1). The goal was to acquire predominantly lacustrine sediments that would preserve an ecological and environmental record of the paleolake, which could then be tied directly to outcrops (both within the paleolake and lake margins), thus linking the paleoclimatic record of the lake to important events in hominin evolution preserved at Olduvai. However, upon recovery of the cores it became clear that paleolake Olduvai was more consistently lacustrine than anticipated based on outcrop studies, for all three core sites. More details on the sedimentology and stratigraphy of the OGCP cores can be found in Stanistreet et al. (2020).

All four cores include significant pyroclastic components, with thick tuffs, thin units within lacustrine sediments, and major pyroclastic flow deposits. Preservation of volcanic glass is poor overall, as glass was commonly degraded and replaced by zeolites and clays within the saline-alkaline lake and groundwater environments of the Olduvai Basin (e.g. Hay and Kyser, 2001; McHenry, 2009, 2010). However,

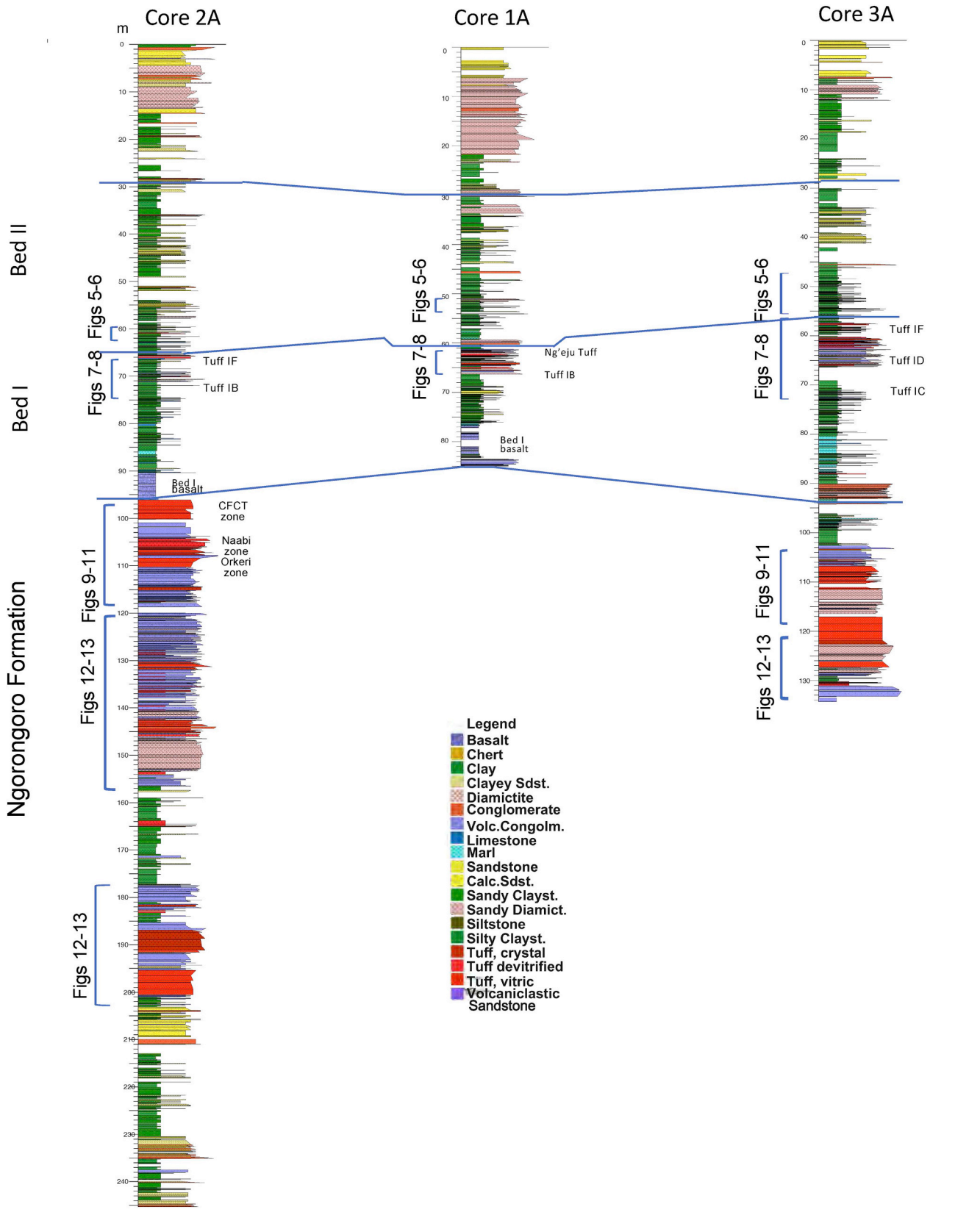

Fig. 3. Core stratigraphy (for OGCP cores 1A, 2A, and 3A). Boundaries between the Ngorongoro Formation, Bed I, and Bed II based on Stanistreet et al. (2020). Tuff-rich intervals of focus for this study are indicated in brackets, showing which figures correspond to each interval. Named marker tuffs and ignimbrites based on the results of the current study.

phenocrysts (including feldspars, augite, and hornblende) are usually preserved, and titanomagnetite and ilmenite are frequently preserved. Existing mineralogical and geochemical fingerprints for the Olduvai tuffs (e.g. McHenry, 2005, 2012; McHenry et al., 2008, 2016; McHenry and Stanistreet, 2018) are based primarily on phenocryst composition because of the lack of glass across much of the basin, and can thus be applied to the heavily altered tuffs intersected in the cores. Fig. 3 shows the stratigraphy of Cores 1A, 2A, and 3A, indicating intervals of lacustrine sedimentation and volcanic deposition.

2.2. The Ngorongoro Volcanic Highlands

The Olduvai Basin is directly adjacent to the Ngorongoro Volcanic Highlands (NVH, to the east and southeast, Fig. 1), which provided pyroclastics to the basin from a succession of volcanoes throughout its history. Its proximity means that in addition to airfall tuffs, its volcanoes also provided pyroclastic surges and flows, and that mass flows and streams transported eroded volcaniclastic materials from the volcanic edifices directly into the basin. The NVH changed in character over time, with different volcanic centers producing different compositions, and active during different intervals. The largely rhyolitic products of Ngorongoro dominate the volcanic record of the newly defined Ngorongoro Formation (exposed in outcrop only in the western gorge, but represented in both OGDP Cores 2A and 3A, and defined in Stanistreet et al., 2020). Ngorongoro Volcano produced a thick fan-delta of volcaniclastic material into the Olduvai Basin during periods of activity, including ignimbrites such as the Naabi, Coarse Feldspar Crystal Tuff (CFCT) equivalent, and ignimbrites exposed on the First Fault to the southeast of the Olduvai Basin and recognized in the oldest outcrop exposures in the western part of Olduvai Gorge. The new cores push this record back even further, as they preserve multiple pulses of volcaniclastic deposits below the level of the Naabi Ignimbrite. More trachytic Olmoti Volcano was the source of the tuffs of Upper Bed I (Tuffs IB through IF, see McHenry et al., 2008). More nephelinitic compositions appear in Bed II, with potential sources at Embagai and Loolmalasin (Mollel and Swisher III, 2012), though Greenwood (2014) found Embagai to be more compositionally similar to Bed III. The changing composition and nature of volcanic deposits at Olduvai helps trace the volcanic evolution of the NVH over time.

2.3. Olduvai tuff markers

Hay (1976) defined and described a series of marker "tuffs" that he used to date and characterize the stratigraphy of Olduvai. He used the term "tuff" loosely, describing sedimentary beds of differing volcaniclastic content, some of which were fairly uncontaminated airfall tuffs, and others of which were mappable lithostratigraphic units with only minor pyroclastic material (e.g. Tuff IIB: McHenry et al., 2016). In this work we will retain Hay's nomenclature for "Tuffs" that are found in both core and outcrop, distinguishing the named markers with a capital "T". These named tuffs, with dates (from Deino, 2012) are shown, in stratigraphic order, in the composite section of Fig. 2. We will also describe new volcaniclastic units, both below the level of the oldest outcrop exposures at Olduvai (the Naabi Ignimbrite in the western gorge), and from higher parts of the core, where some tuffs are found that have not been previously identified compositionally from outcrop.

2.4. Tuff fingerprinting using phenocrysts

The saline-alkaline nature of paleolake Olduvai, and the inferred groundwater environment of the Olduvai Basin, limits the preservation of volcanic glass. Most tuffs are now dominated by zeolites and clays replacing the original glass (McHenry, 2009, 2010). By contrast, phenocrysts are largely preserved (except for oxides such as titanomagnetites, which are often absent from the most altered paleolake tuff samples), though in some cases overgrowths of authigenic K-feldspar surround original volcanic anorthoclase in the most lacustrine samples. Fortunately, these rims can be easily avoided when conducting electron probe microanalysis (EPMA). The limited preservation of volcanic glass limits the techniques that can be applied to geochemically "fingerprint" the tuffs, a process that most often involves glass compositions. A multiple-technique approach pioneered by McHenry (2004, 2005, 2012), using a combination of stratigraphic order, mineral assemblage, and major and minor element compositions of the phases that are preserved (typically feldspar, augite, +/− hornblende, +/− oxide (titanomagnetite and/or ilmenite), rarely volcanic glass), allows for at least locally applicable fingerprinting.

3. Methods

3.1. Core sampling

Vertical boreholes OGCP-1A, 2A, and 3A were drilled at three different sites in the Olduvai Basin (Fig. 1) targeting the purported depocenters for the paleolake during different stratigraphic intervals, and a 23° inclined borehole was additionally drilled (3B) for paleomagnetic analysis. Cores were retrieved in 3 m intervals (6 cm core diameters), and the core segments were then cut into ~150 cm increments. For example, for the 15th interval collected for core 2A, the core would be broken down into: 2A-15Y-1 (1.53 m), 2A-15Y-2 (1.54 m), and 2A-15Y-3 (0.14 m corecatcher). 574.45 m of core was retrieved from the four boreholes combined, with 94.1% recovery overall. The stratigraphies of Cores 1A, 2A, and 3A are shown in Fig. 3, and explained in more detail in Stanistreet et al. (2020). This figure also highlights the core intervals of greatest focus for the present tephrostratigraphic study.

Tuffs were sampled during the initial core sampling "party" at LacCore, the National Lacustrine Core Facility at the University of Minnesota- Twin Cities. For thinner tuffs, the entirety of the tuff was sampled from the working half of the core for $^{40}Ar/^{39}Ar$ dating, and the < 230 μm size fraction remaining after $^{40}Ar/^{39}Ar$ dating sample preparation was provided for tuff geochemistry. For thicker tuffs, a separate sample was collected just for tuff geochemistry (~4–10 g of material), adjacent to the sample collected for $^{40}Ar/^{39}Ar$ dating. Appendix 1 lists all samples analyzed in this study, their depth (meters below surface (mbs) for the top of each sample), whether the sample analyzed was a split of a $^{40}Ar/^{39}Ar$ dating sample, a brief description of the units sampled, and notes on their mineral compositions.

3.2. Laboratory analysis

Samples were air dried, gently disaggregated using a ceramic mortar and pestle, and then sieved. The 60–100 μm size fraction was then cleaned using a dilute (4%) HF solution in a sonicator for 1 min, followed by at least three rounds of rinsing in deionized water until the decanted water was no longer muddy, then dried under a heat lamp. Individual glass shards and phenocrysts were hand picked and mounted in holes drilled into a 1-in. diameter acrylic disc. Around 15–20 grains of each target mineral (feldspar, augite, titanomagnetite/ilmenite for most samples; hornblende for many, and glass where available), along with a few grains of other minerals if present (e.g. andradite, perovskite, biotite, sphene, olivine, apatite, quartz) were selected. These were mounted in epoxy, then polished to expose the interiors of the grains, with a final grit size of 1 μm.

Microprobe mounts where carbon coated and then analyzed by electron probe microanalysis (EPMA) at University of Wisconsin-Madison, most often using a Cameca S-Five. Phase identifications were confirmed using energy dispersive spectroscopy (EDS), and then phase-specific analytical routines were used to analyze each type, using wavelength dispersive spectroscopy (WDS). Check samples (including feldspar, augite, hornblende, glass, and titanomagnetite) were analyzed at the start of every EPMA run, and calibrations were adjusted accordingly to ensure consistency between runs. Specific methods

Table 1
Sample list, with phases analyzed and observed.

Sample	MBS (top)	Augite	HB	Plag	Anclas	K-spar	Ti-mag	Ilmenite	Glass	Quartz	Andradite	Sphene	Perovskite	Apatite	Olivine	Biotite	Aenig	Calcite	Pyrite	Chromite
1A-2Q1-28-30	2.93	XX	+	+	+	+	XX	-	-	X	XX	+	-	+	-	+	-	-	-	-
1A-2Q2-58-60	4.23	XX	+	+	-	X	XX	-	-	+	X	-	+	+	-	-	-	-	-	-
1A-15Q2-86-88	43.60	XX	XX	X	X	-	XX	-	-	+	-	-	-	-	-	-	-	+	-	-
1A-19Q1-47-48	51.52	XX	+	XX	-	-	+	-	-	+	-	-	-	-	-	-	-	-	-	-
1A-19Q1-48-53	51.55	XX	-	XX	-	-	X	-	-	+	-	-	-	+	-	-	-	-	-	+
1A-19Q1-54-55	51.59	XX	+	XX	-	-	+	-	-	+	-	-	-	-	-	-	-	-	-	-
1A-19Q1-82-82	51.87	XX	X	X	+	-	XX	-	-	-	-	+	+	-	-	-	-	-	-	-
1A-19Q1-83-85	51.88	XX	X	XX	+	-	XX	-	-	+	-	-	-	-	-	-	-	-	-	-
1A-19Q2-85-92	52.98	XX	X	XX	XX	+	XX	-	-	+	-	-	-	-	-	-	-	-	-	-
1A-20Q1-79.5-81	54.86	XX	-	-	X	-	+	-	-	+	-	-	-	-	-	-	-	+	-	-
1A-20Q1-80-83	54.85	XX	-	+	-	-	X	-	-	X	-	-	-	-	-	-	-	X	-	-
1A-20Q2-39-41	55.63	XX	-	+	+	-	X	+	-	X	-	-	-	-	-	-	-	X	-	-
1A-22Q1-127-130	61.32	XX	XX	XX	-	-	XX	-	+	-	-	-	-	-	-	-	-	-	-	-
1A-22Q2-10-12	61.54	XX	XX	XX	-	-	XX	-	-	-	-	-	-	X	-	-	-	-	-	-
1A-22Q2-46-48	61.90	XX	XX	XX	-	-	XX	+	-	-	-	-	-	-	-	-	-	-	-	-
1A-22Q2-63-69	62.08	XX	XX	XX	X	-	XX	+	-	-	-	-	-	-	-	-	-	-	-	-
1A-22Q2-89-90.5	62.33	X	-	+	+	-	+	-	-	XX	-	-	-	-	-	-	-	XX	-	-
1A-22Q2-103-105	62.47	XX	+	-	XX	-	XX	-	-	-	-	-	-	-	-	-	-	-	-	-
1A-22Q2-118-120	62.62	XX	-	XX		-	XX	-	-	-	-	-	-	-	-	-	-	-	-	-
1A-22Q2-132-133	62.76	XX	-	-	XX	-	XX	-	-	-	-	-	-	-	-	-	-	-	-	-
1A-22Q3-8-10	62.87	XX	+	-	XX	-	XX	-	-	-	-	-	-	-	-	-	-	+	-	-
1A-23Q1-54.5-56	63.61	XX	+	-	XX	-	+	+	-	-	-	-	-	-	-	-	-	-	-	-
1A-23Q1-134-136	64.39	XX	+	XX	XX	-	XX	-	-	-	-	-	-	-	-	-	-	-	-	-
1A-23Q2-62.5-63.5	65.04	XX	+	+	XX	-	XX	-	-	-	-	-	-	-	-	-	-	-	-	-
1A-23Q2-70-72	65.11	XX	-	-	XX	-	XX	-	-	-	-	-	-	-	-	-	-	-	-	-
1A-23Q2-119-121	65.60	XX	-	X	XX	-	XX	-	-	-	-	-	-	-	-	-	-	-	-	-
1A-25Q1-100-112	70.04	XX	X	XX	XX	-	XX	-	-	-	-	-	-	-	-	-	-	-	-	-
1A-25Q1-112-114	70.11	XX	X	X	XX	-	+	+	-	-	-	-	-	-	-	-	-	-	+	-

Sample list, continued, Core 2A (upper)

Sample	MBS (top)	Augite	HB	Plag	Anclas	K-spar	Ti-mag	Ilmenite	Glass	Quartz	Andradite	Sphene	Perovskite	Apatite	Olivine	Biotite	Aenig	Calcite	Pyrite	Chromite
2A-25Y2-39-40	59.62	XX	X	+	X	-	X	-	-	-	-	-	-	-	-	-	-	+	-	-
2A-25Y2-55-59	59.72	XX	X	X	+	+	XX	+	-	X	-	-	-	-	-	-	-	-	-	+
2A-25Y2-70-70.5	59.85	XX	-	+	X	+	+	-	-	+	-	-	-	-	-	-	-	-	-	+
2A-26Y1-91-97	60.94	X	-	X	XX	+	-	-	-	+	-	-	-	-	-	-	-	X	-	-
2A-26Y1-111-112	61.11	XX	+	X	X		X	-	-	+	+	-	-	-	-	-	-	-	-	-
2A-27Y1-71-73	64.64	XX	-	-	+	+	X	-	-	+	-	-	-	+	-	-	-	+	-	+
2A-27Y1-80-83	64.81	X	X	-	+	+	+	+	-	-	-	-	-	-	-	-	-	X	-	-
2A-28Y1-80-83	65.70	XX	X	-	XX	+	XX	X	-	-	-	-	-	-	-	-	-	-	-	-
2A-28Y2-10-12	65.89	X	X	-	XX	+	XX	-	-	-	-	-	-	-	-	-	-	-	-	-
2A-30Y1-12-18	69.15	XX	X	XX	X	-	-	-	-	-	X	-	-	-	-	-	-	X	-	+
2A-30Y1-59-65	69.62	XX	XX	XX	+	-	X	X	-	-	-	-	-	-	-	-	-	X	-	X
2A-30Y1-93-95	69.93	XX	XX	XX	-	-	X	X	X	+	-	-	-	-	-	-	-	-	-	-
2A-30Y1-105-107	70.05	XX	+	XX	-	-	X	X	-	-	-	-	-	-	-	-	-	-	-	-
2A-30Y1-111-113	70.11	XX	XX	XX	X	-	X	-	-	-	-	-	-	-	-	-	-	-	-	-
2A-30Y2-70-72	71.14	XX	+	+	XX	-	-	-	+	-	-	-	-	-	-	-	-	-	-	-
2A-30Y2-78-79	71.22	XX	-	-	XX	-	-	-	-	-	-	-	-	-	-	-	-	-	-	-
2A-30Y3-11-13	71.97	XX	-	-	XX	-	-	-	-	-	-	-	-	-	-	-	-	-	-	-
2A-31Y1-0-5	72.03	XX	+	+	XX	+	-	+	-	-	-	-	-	-	-	-	-	-	-	-
2A-38Y2-91-93	95.29	XX	-	XX	X	-	XX	+	-	-	-	-	-	-	-	-	-	-	-	-
2A-39Y1-20-25	96.20	XX	-	+	XX	-	+	XX	-	-	-	-	+		-	-	-	-	-	-

(*continued on next page*)

Table 1 (*continued*)

Sample list, continued, Core 2A (upper)

Sample	MBS (top)	Augite	HB	Plag	Anclas	K-spar	Ti-mag	Ilmenite	Glass	Quartz	Andradite	Sphene	Perovskite	Apatite	Olivine	Biotite	Aenig	Calcite	Pyrite	Chromite
2A-39Y1-133-135	97.34	XX	-	-	XX	-	XX	+	-	-	-	-	-	-	-	-	-	-	-	-
2A-39Y2-23-24	97.65	XX	+	-	XX	-	XX	+	+	-	-	-	-	-	-	-	-	-	-	-
2A-39Y2-68-71	98.15	XX	-	+	XX	-	XX	+	-	+	-	-	-	-	-	-	-	-	-	-

Sample list, continued, Core 2A (lower)

Sample	MBS (top)	Augite	HB	Plag	Anclas	K-spar	Ti-mag	Ilmenite	Glass	Quartz	Andradite	Sphene	Perovskite	Apatite	Olivine	Biotite	Aenig	Calcite	Pyrite	Chromite
2A-42Y2-124-126	104.65	XX	+	-	XX	-	X	+	XX	+	-	-	-	-	-	-	+	-	-	-
2A-43Y1-126-128	106.23	XX	-	-	XX	-	-	+	XX	-	-	-	-	-	-	-	+	-	-	-
2A-43Y2-47-49	106.87	X	-	-	XX	-	+	+	XX	-	-	+	-	-	-	-	-	-	-	-
2A-43Y2-77-80	107.16	XX	-	-	XX	-	+	X	XX	-	-	-	-	-	-	-	-	-	-	-
2A-44Y1-74-76	108.74	XX	-	-	XX	-	X	X	-	-	-	-	-	-	-	-	-	-	-	-
2A-44Y2-14-16	109.48	XX	+	-	XX	-	X	+	-	-	-	-	-	-	-	-	-	-	-	-
2A-44Y2-51-53	109.85	XX	-	-	XX	-	X	X	-	-	-	-	-	-	-	-	-	-	-	-
2A-44Y2-106-108	110.40	XX	-	-	XX	-	X	X	XX	-	-	-	-	-	-	-	-	-	-	-
2A-44Y2-114-116	110.48	+	XX	+	XX	-	-	-	+	-	-	-	-	-	-	-	-	-	-	-
2A-44Y2-121-123	110.55	+	+	-	XX	-	+	-	XX	-	-	-	-	-	-	-	-	-	-	-
2A-46Y1-107-125	115.11	XX	-	+	XX	-	X	X	XX	-	-	-	-	-	-	-	-	-	-	-
2A-48Y2-35-44	121.85	XX	-	XX	-	-	-	+	XX	-	-	-	-	-	-	-	-	-	-	-
2A-50Y2-75-89	128.25	XX	-	-	XX	-	+	X	XX	-	-	-	-	+	-	-	-	-	-	-
2A-51Y2-68-78	131.15	XX	-	-	XX	-	X	X	XX	-	-	-	-	-	-	-	-	-	-	-
2A-52Y1-101-104	132.98	X	-	-	XX	-	+	-	XX	-	-	-	-	-	-	-	-	-	-	-
2A-52Y2-17-28	133.65	XX	-	-	XX	-	X	X	XX	-	-	-	-	-	+	-	-	-	-	-
2A-55Y2-127-130	143.73	XX	+	-	XX	-	XX	+	X	-	-	-	-	-	-	-	-	-	-	-
2A-57Y2-72-74	149.17	X	+	-	XX	-	X	+	X	-	-	-	-	-	+	-	-	-	-	-
2A-59Y2-82-84	152.45	XX	-	-	XX	-	XX	-	XX	-	-	-	-	-	-	-	-	-	-	-
2A-61Y1-48-51	156.50	XX	X	X	XX	-	XX	+	-	-	-	-	-	+	-	-	-	-	-	-
2A-68Y1-100-108	178.04	+	-	-	XX	-	+	XX	X	-	-	-	-	-	-	-	-	+	-	-
2A-69Y23941	181.85	XX	-	-	XX	-	+	+	-	-	-	-	-	-	-	-	-	-	-	-
2A-72Y2-11-13	190.53	XX	-	-	XX	-	XX	-	-	-	+	-	-	-	-	-	-	-	-	-
2A-72Y2-24-26	190.66	XX	XX	-	XX	-	X	+	-	-	-	-	-	-	-	-	-	-	-	-
2A-74Y2-96-98	196.06	XX	-	+	XX	-	X	X	XX	-	-	-	-	-	-	-	-	-	-	-
2A-75Y2-128-133	200.76	XX	-	X	XX	-	XX	-	+	-	-	-	-	-	-	-	-	-	-	-
2A-76Y2-14-16	202.60	XX	X	X	XX	-	XX	-	-	X	+	-	-	-	-	+	-	-	-	-

Sample list, continued, Cores 3A and 3B

Sample	MBS (top)	Augite	HB	Plag	Anclas	K-spar	Ti-mag	Ilmenite	Glass	Quartz	Andradite	Sphene	Perovskite	Apatite	Olivine	Biotite	Aenig	Calcite	Pyrite	Chromite
3A-4Y1-88-95	7.02	XX	+	X	+	X	X	-	-	X	XX	-	-	+	-	-	-	-	-	-
3A-19Y2-16-18	46.06	XX	XX	-	X	-	+	-	-	-	-	-	-	-	-	-	-	-	-	-
3A-21Y3-2-5	50.12	XX	-	+	+	-	-	-	-	-	-	-	-	-	-	-	-	-	-	+
3A-21Y3-58-62	50.68	XX	-	+	+	-	-	-	-	-	-	-	-	-	-	-	-	-	-	-
3A-22Y1-29-31	51.40	XX	-	-	-	-	-	-	-	+	-	-	-	-	-	-	-	-	-	+
3A-22Y1-32-35	51.42	XX	-	X	-	-	-	-	-	+	-	-	-	-	-	-	-	-	-	-
3A-22Y1-110-111	52.20	XX	-	X	X	-	-	-	+	-	-	-	-	-	X	-	-	-	-	-
3A-22Y1-117-118	52.28	XX	X	X	X	-	+	X	-	-	+	-	-	-	-	-	-	-	-	+
3A-22Y1-136-138	52.46	XX	X	X	XX	-	+	-	-	+	-	-	-	-	-	-	-	+	-	-
3A-22Y2-0-1	52.51	XX	-	X	XX	-	X	-	-	-	-	-	-	-	-	-	-	-	-	-
3A-22Y2-20-21	52.71	XX	-	X	-	-	+	-	+	XX	-	-	-	-	-	-	-	+	-	-
3A-22Y2B-53-58	53.06	XX	-	XX	-	X	-	-	-	X	-	-	-	-	-	-	-	-	-	X

(*continued on next page*)

Table 1 (*continued*)

Sample list, continued, Cores 3A and 3B

Sample	MBS (top)	Augite	HB	Plag	Anclas	K-spar	Ti-mag	Ilmenite	Glass	Quartz	Andradite	Sphene	Perovskite	Apatite	Olivine	Biotite	Aenig	Calcite	Pyrite	Chromite
3A-22Y2-85-89	53.36	XX	-	X	+	-	-	-	-	+	-	-	+	-	-	-	-	XX	-	+
3A-23Y1-37-39	54.45	XX	+	X	X	-	+	-	-	-	-	-	-	-	-	-	-	+	-	-
3A-24Y1-46-48	57.56	XX	-	+	XX	-	XX	+	-	-	-	-	-	-	-	-	-	-	-	-
3A-24Y1-75-77	57.85	XX	XX	-	XX	+	X	-	-	-	-	-	-	-	-	-	-	-	-	-
3A-24Y2-28-30	58.71	X	X	+	XX	-	-	-	-	-	-	-	-	-	-	-	-	X	-	-
3A-25Y1-33-35	60.43	XX	XX	XX	X	-	XX	-	-	-	-	-	-	-	-	-	-	-	-	-
3A-25Y1-58-61	60.68	XX	-	+	XX	-	XX	-	-	-	-	-	-	-	-	-	-	-	-	-
3A-25Y1-112-114	61.22	XX	+	+	X	-	XX	-	-	-	-	-	-	-	-	-	-	-	-	-
3A-25Y1-132-134	61.42	XX	-	+	XX	-	XX	-	-	-	-	-	-	-	-	-	-	-	-	-
3A-25Y2-36.5-37.5	61.86	XX	+	+	XX	-	XX	-	-	-	-	-	-	-	-	-	-	-	-	-
3A-25Y2-61-63	62.10	XX	+	-	XX	-	XX	-	-	+	-	-	-	-	-	-	-	-	-	-
3A-25Y2-119-121	62.68	XX	XX	-	XX	-	XX	-	-	-	-	-	-	-	-	-	-	-	-	-
3A-26Y1-89-91	63.98	XX	X	+	XX	-	XX	-	-	-	-	-	-	-	-	-	-	-	-	-
3A-26Y1-117-119	64.25	XX	-	+	XX	-	+	+	-	-	-	-	-	-	-	-	-	-	-	-
3A-26Y2-36-42	64.94	XX	-	-	XX	-	XX	-	-	-	-	-	-	-	-	-	-	-	-	-
3A-26Y2-107-109	65.61	XX	-	-	XX	-	XX	-	-	-	-	-	-	-	-	-	-	-	-	-
3A-26Y2-146-149	66.01	XX	-	X	XX	-	XX	-	-	-	-	-	-	-	-	-	-	-	-	-
3A-26Y3-0-2	66.02	XX	-	XX	X	-	XX	-	-	-	-	-	-	-	-	-	-	-	-	-
3A-28Y2-107-111	71.65	XX	X	X	XX	-	X	+	-	-	-	-	-	-	-	-	-	-	-	-
3A-28Y2-137-138	71.95	XX	-	+	XX	-	+	-	-	-	-	-	-	-	-	-	-	-	X	-
3A-33Y1-19-20	84.25	X	+	+	-	+	-	-	-	-	-	-	-	-	-	-	-	-	XX	+
3A-33Y1-51-53	84.51	XX	+	XX	+	+	-	-	-	+	XX	-	+	-	-	-	-	-	+	-
3A-33Y1-54.5-56	84.54	XX	+	+	-	+	+	-	-	+	XX	-	-	-	-	-	-	-	+	-
3A-38Y2-95.5-97.5	98.47	-	XX	X	XX	-	-	-	+	+	-	-	-	-	-	-	-	-	-	-
3A-38Y2-128-130	98.79	-	-	+	X	-	-	-	-	-	-	-	-	-	-	-	-	+	XX	-
3A-41Y1-80-82	105.87	-	-	-	XX	-	-	-	XX	-	-	-	-	-	-	-	-	-	-	-
3A-41Y1-99-101	106.06	+	-	-	XX	-	+	+	XX	-	-	-	-	-	-	-	-	-	-	-
3A-41Y2-28-30	106.82	XX	-	+	XX	-	X	+	XX	+	+	-	-	-	-	-	+	-	-	-
3A-50Y2-39-47	130.93	XX	-	-	XX	-	XX	+	XX	-	-	-	-	-	-	-	-	-	-	-
3B-19Y1-45-51	54.38	XX	-	+	+	-	+	+	-	-	-	-	-	-	-	-	-	-	-	-
3B-19Y2-54-56	55.49	XX	X	X	XX	-	+	-	-	X	-	-	-	-	-	-	-	-	-	-
3B-19Y3-6-8	56.04	XX	+	X	-	-	-	-	-	-	-	-	-	-	-	-	-	-	-	X
3B-25Y1-61-62	72.48	XX	+	-	XX	-	XX	-	-	-	-	-	-	-	-	-	-	-	-	-
3B-34Y2-47-50	97.86	-	-	X	-	-	-	-	-	-	-	-	-	-	-	-	-	-	-	-
3B-49Y2-61-63	142.38	XX	-	-	XX	-	XX	X	XX	-	-	-	-	-	-	-	-	-	-	-

XX = abundant, X = rare to common, + = present, − = absent.

(including instrument details, beam parameters, standards, and test samples) are reported in McHenry et al. (2016). Every grain was first examined using backscattered electron (BSE) imagery to assess the potential for compositional zonation and to avoid inclusions, and a single point was analyzed for each. As was observed in McHenry (2005), where multiple points were measured for each grain, compositional zonation and heterogeneity appear to be minimal in phenocrysts from Olduvai tephra. Points were positioned near the center of grains, unless another position was preferable to avoid inclusions or cracks, though due to the polishing geometry, it is still possible that some analyzed points were near edges above or below.

Data quality was assessed by calculating formula units to an appropriate number of oxygens to ensure reasonable stoichiometry, and excluding analyses with exceptionally low totals (< 90% for glass and titanomagnetites). For each sample, clearly distinct populations of each phase (e.g. plagioclase vs. anorthoclase, high-Na augite from low-Na augite) were identified and treated as separate populations. An average was calculated for each population, along with a standard deviation.

The presence, absence, and relative abundance of different mineral phases for each sample was estimated based on the prepared mounts, and each phase was confirmed using EDS observations (even when no WDS data were collected). Phases for which 10+ grains were mounted are classified as "abundant" (XX in Table 1), those for which only one or two grains were found and mounted are classified as "present" (+ in Table 1), with amounts between those two extremes considered "rare to common" (X in Table 1). While the sample mounting procedure introduces some bias to this determination (since we attempt to find and mount ~15 grains of the target phases augite, feldspar, hornblende, and glass, if present), especially for the less abundant phases, it provides a reasonable estimate for their comparative rarity that should be internally consistent for this data set.

4. Results

The results comprise major and minor element compositions for all major phenocrysts present within each sample, where possible from 15 to 17 grains or shards of each. Minor or non-target phenocrysts may be represented by a smaller number of grains analyzed, or a simple observation of presence/absence (thus the EPMA analysis was used only to confirm the identification of the phase). Table 1 tabulates the presence and qualitative relative abundances of each phase. Notes on the mineral compositions measured for each sample, along with a brief sample description, are provided in Appendix 1. All analyses of core samples that meet the data quality requirements outlined above are reported in Appendices 2–15, organized by phase (augite, hornblende, feldspar, titanomagnetite, glass) and stratigraphic interval (Bed II, Bed I (above the basalts), and Lower Bed I/Ngorongoro Formation (below the basalts)). Previously unpublished EPMA data for outcrop samples equivalent to the upper part of the Ngorongoro Formation, used for comparison, are provided in Appendices 16–19.

Because of the large volume of data, the core tuffs have been subdivided based on stratigraphic interval and are only compared within each interval in the data plots to follow. These intervals are: Bed II, Bed I (above Bed I basalts, through Tuff IF), the upper part of the new Ngorongoro Formation (Stanistreet et al., 2020) with potential outcrop correlatives (Orkeri Ignimbrite equivalents up to the base of the Bed I Basalt), and the older part of the Ngorongoro Formation with no outcrop equivalents (below 120 mbs in Core 2A). The intervals of focus are indicated in brackets on Fig. 3. Not every sample is plotted for each data plot, especially where multiple samples of similar composition were analyzed over an interval (e.g. the Tuff IE and Ng'eju compositional zones in Core 3A). In these cases, a single sample that best represents the target composition (free from contaminants, sufficient grains analyzed for each target phase, etc.) was chosen for plotting, however data from all samples analyzed are reported in the appendices. The positions of all samples analyzed within the target intervals are shown on the stratigraphic columns for Beds I and II, with plotted samples indicated by their symbols. To accentuate specific comparisons within more restricted stratigraphic intervals, a smaller number of more closely spaced samples was plotted.

Glass is almost universally absent in tuffs from all cores in Beds I and II, but usually present in tuffs within the older Ngorongoro Formation. Titanomagnetite is also often absent in these more altered, lacustrine tuffs. This is consistent with outcrop exposures, where prior studies have found that glass is replaced by a combination of clays and zeolites in tuffs emplaced within the saline-alkaline lake (e.g. Hay and Kyser, 2001; McHenry, 2009, 2010). Fresh glass is only occasionally observed and titanomagnetite is usually preserved in lake margin settings, but since the coring targeted the lake depocenters, these were not expected to be abundant in the cores. Feldspar (a range of plagioclase, anorthoclase, and sanidine compositions) and augite are present in almost all samples. Hornblende is present in specific units or intervals, and its presence or absence thus helps to identify particular tuffs or compositional "zones" within the volcanic and volcaniclastic strata. Other minerals observed more rarely (though they can be abundant in specific intervals) include andradite garnet, titanite (sphene), perovskite, apatite, olivine, aenigmatite, and chromite. When present, iron oxide grains are most often titanomagnetite and/or ilmenite. The presence of calcite and/or quartz typically reflects contamination by non-pyroclastic materials (and is often associated with more rounded, detrital mineral grains), although primary volcanic quartz is likely in some rhyolites from the Ngorongoro Formation.

Some trends can be observed in tuff mineral assemblages throughout the core, tracking changes in the volcanic source areas over time. The volcanic units (tuffs and pyroclastic flow deposits) of the newly defined Ngorongoro Formation (and likely sourced from Ngorongoro Volcano) are dominated by rhyolites, with rhyolitic glass, anorthoclase to sanidine feldspar, augite, titanomagnetite and/or ilmenite, and (more rarely) hornblende or aenigmatite. Tuffs within Bed I, more likely sourced from Olmoti Volcano, are more trachytic, though glass is rarely preserved in the core samples from this interval. Within Bed I, feldspar is most often anorthoclase, though specific tuffs are dominated by plagioclase instead. Augite is present in all Bed I tuffs, while hornblende is restricted to specific tuffs. Titanomagnetite is present in some samples, though its presence and absence is likely related to preservation rather than original composition, similar to glass. The volcanic and volcaniclastic record of Bed II is much sparser, with tuffs largely absent from the upper sections and thin, altered, and contaminated in the lower sections. In these lower Bed II tuffs and volcaniclastic units, glass is absent and feldspar typically covers a broad range of compositions from anorthoclase to plagioclase, though some individual tuffs (or samples) show a more restricted range. A distinctive high-Ca plagioclase composition is observed in Cores 1A and 3A during a short interval (with multiple units); the same samples contain augite with elevated Mg (Fig. 4). Tuffs were not observed or sampled in the Bed III/IV/Masek intervals, and tuffs in the Ndutu Beds yield a significantly different assemblage than the lower beds (less feldspar, abundant augite, titanomagnetite, and andradite garnet, accessory titanite, perovskite, apatite, and biotite).

5. Proposed correlations

The EPMA results for the target phases analyzed for each sample were plotted against a database of published and unpublished analyses of tuffs from Olduvai outcrops (McHenry, 2005, 2012; McHenry et al., 2016; Habermann et al., 2016; McHenry and Stanistreet, 2018), and against other tuffs from the same general interval within the cores, to look for similarities. Such similarities, or distinctive properties, were noted for each phase in each sample. Correlations are proposed for when: (1) the stratigraphic equivalence is reasonable, (2) the mineral assemblage is consistent, (3) for each phase analyzed, most grains plot within the same field for all elements (this allows for some outliers/

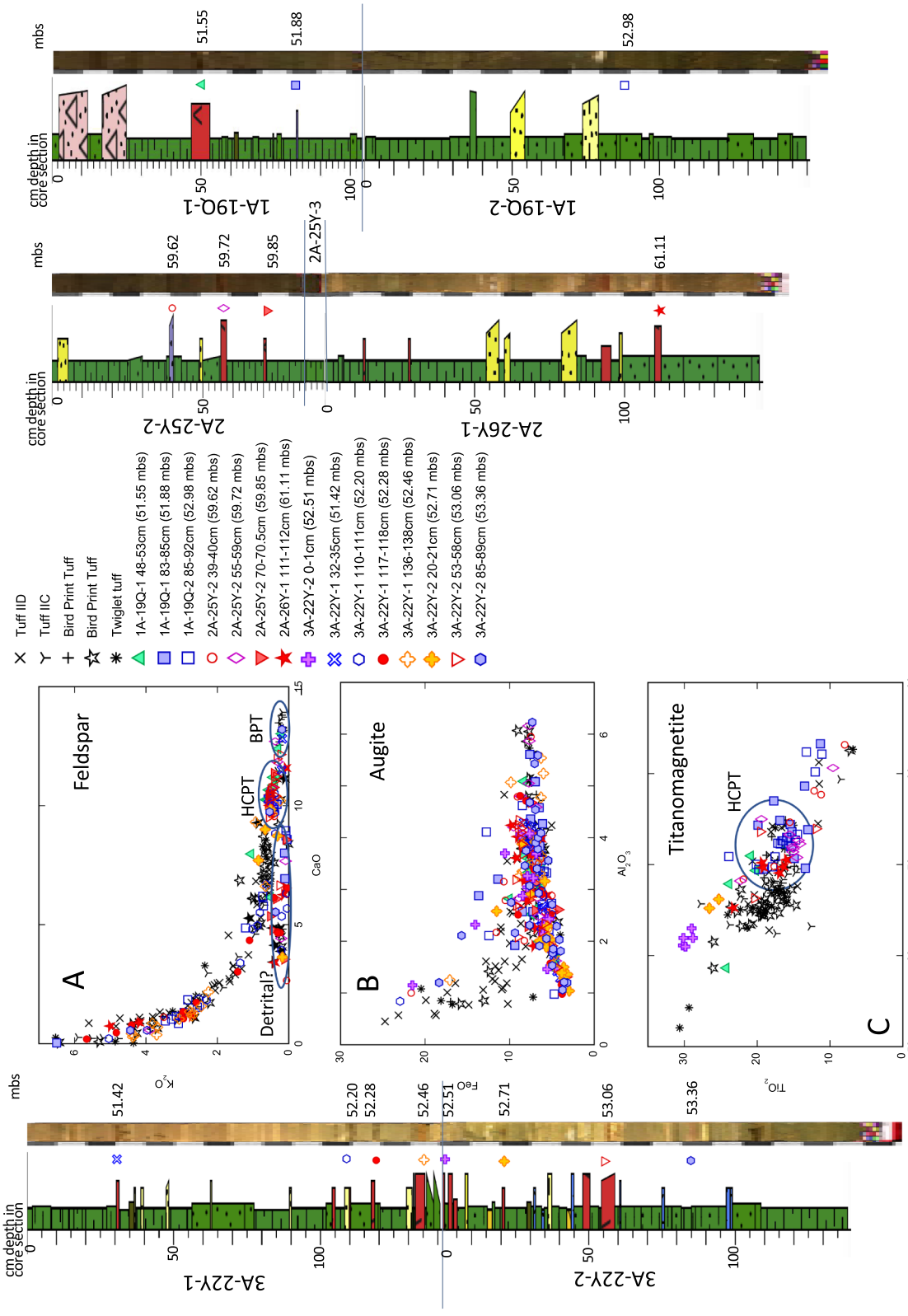

Fig. 4. Measured core sections, and associated data plots, for Middle Bed II. Key for colors (indicative of facies) in Fig. 3. The position of each sample within this core depth range for Cores 1A, 2A, and 3A is indicated next to the photograph of the core segment, with its depth (in meters below surface, or mbs). Samples included in the plots in this figure are further indicated by their symbol, between the core photograph and the associated measured stratigraphic section. Blue circles highlight the range of composition of the main populations for select marker tuffs (note that some individual grains fall outside this range). A. Feldspar composition, K_2O vs. CaO. Black symbols are for Bed II geochemical "type" samples reported in McHenry et al., 2016, colored symbols represent core samples. A new high calcium plagioclase tuff (HCPT) composition, identified in all three cores but not in outcrop, is offset from outcrop samples of the Bird Print Tuff (BPT) in their slightly lower CaO. B. Augite composition, Al_2O_3 vs. FeO. C. Titanomagnetite composition, TiO_2 vs. FeO, for samples that preserve titanomagnetite. The HCPT samples plot together with higher FeO than most Bed II tuffs, though overlapping with the BPT. (For interpretation of the references to color in this figure legend, the reader is referred to the web version of this article.)

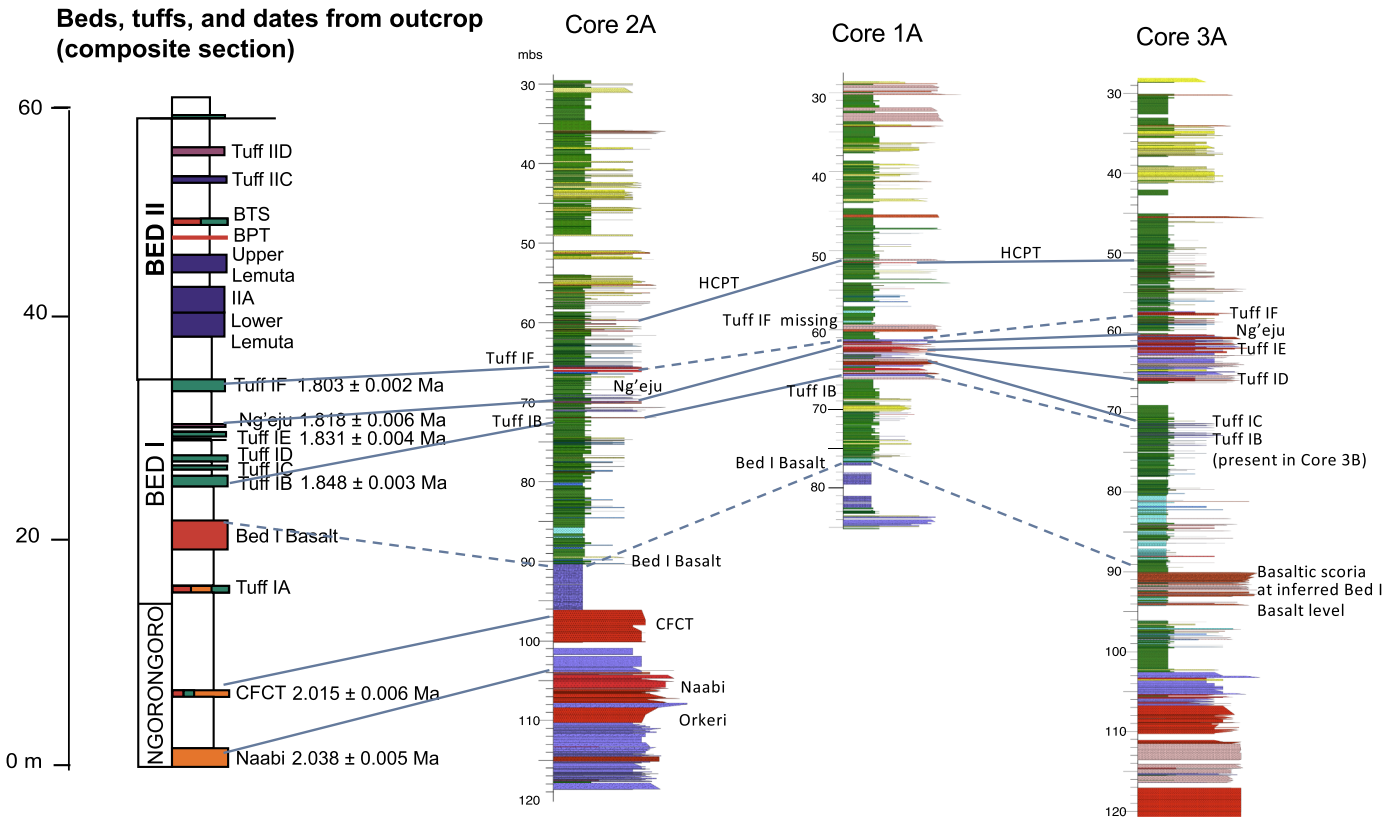

Fig. 5. Proposed correlations. Composite Olduvai stratigraphy, showing positions and dates (from Deino, 2012) of marker tuffs, drawn next to core stratigraphic sections from 30 to 120 mbs. Solid lines represent correlations based on tephra composition (reported in this paper), dashed lines indicate inferred correlations (e.g. top of Bed I basalt in outcrop, Cores 2A and 1A, provisionally correlated to basaltic scoria-bearing layer in Core 3A). Tephra colors from composite strat section from Fig. 2, colors and fill patterns for cores from Fig. 3.

detrital contamination), and (4) this combination of stratigraphic position, mineral assemblage, and phase compositions is unique to a particular tuff or interval of tuffs within the Olduvai strata. Correlations based on multiple phases, and for units with unique "fingerprints," are considered to be stronger. The main proposed correlations are presented in Table 2, where the colors correspond to the core. The "quality" of the correlation is indicated by *** (highest certainty), ** (likely), and * (questionable). "Questionable" samples are those for which only a single phase can be used (which does not allow for confirmation), or where there is some discrepancy between the sample and previously described "type" samples (e.g. the presence of hornblende in a sample from a unit in which hornblende was previously described as rare, or an unexpected stratigraphic position). Samples for which no outcrop equivalent is proposed (i.e., those compositions which are so far only known from the cores), are not assigned a quality mark. The evidence for the correlation (e.g. the phases that support the comparison) are noted, along with specific reasons for uncertainty (e.g. lack of corroborating minerals). Further details on mineral compositions for all samples, including those for which no correlations are proposed, are presented in Appendix 1. The main correlations proposed in this study are also shown in Fig. 5.

It should be noted that "tuffs" at Olduvai, following Hay (1976), include primary airfall and reworked deposits, which contain differing amounts of actual tephra material. In this study, samples were collected from volcaniclastic sandstones in addition to actual tuffs, to identify compositional "zones" even where primary tuffs were not preserved. McHenry et al. (2013) introduced this approach to the Olduvai tephrostratigraphic record. In some intervals of the core (where volcaniclastic units were frequent), this results in multiple, closely-spaced samples with similar compositions, or where the primary assemblage is diluted by other detrital contaminants. This complicates fingerprinting, compared to tephrostratigraphic studies elsewhere that rely solely on primary airfall tuffs.

Units are described in descending order as they were originally described during core analysis, and which presents intervals with known outcrop analogs (where correlations are possible) first, followed by newly discovered older deposits with no local outcrop equivalents.

5.1. Bed II tuffs

None of the named marker tuffs known from outcrop from Bed II (Tuff IIA, "Twiglet," Tuff IIB, Bird Print Tuff (BPT), Tuff IIC, or Tuff IID) are geochemically or mineralogically confirmed in any of the cores. This is largely due to the lack of tuffs observed in the cores for the upper part of Bed II, but also likely due in part to the difficulty, even in outcrop samples, of distinguishing between these various units compositionally. Most Lower Bed II tuffs (other than the BPT) have similar, overlapping ranges of augite compositions and a wide compositional range of feldspars with both high- and low-K anorthoclase and plagioclase within individual samples of these tuffs (McHenry et al., 2016; McHenry and Stanistreet, 2018). Many of the tuffs identified in Bed II from the core samples are very thin (~1 cm thick) and preserved within the saline-alkaline lacustrine sediments, thus titanomagnetite is rarely preserved and no glass is present. Samples were small, which did not provide much material from which to pick mineral grains, thus adequate numbers of feldspar crystals were not always available. Abundant calcite and quartz within the prepared samples also reveal significant contamination of these "tuff" samples with detrital material from the surrounding sediment.

5.1.1. Tuff IID

Tuff IID is one of the most widespread markers in Bed II (and the

Table 2
Proposed correlations, Bed II.

Unit	MBS	Quality*	Core	Interval	Justification
Tuff IID??	46.06	*	3A-19Y2	16-18	HB consistent with Tuff IID and above (unlike HB from tuffs in lower Bed II). Augite consistent with Tuff IID (but not exclusive). Few feldspar, no TiMag to double check.
High-Ca Plag Tuff (HCPT)	51.52		1A-19Q1	47-48	Characteristic high-Ca plagioclase (10-12% CaO), Augite range trends towards high Mg, low Al, Fe4
	51.55		1A-19Q1	48-53	Characteristic high-Ca plagioclase (10-12% CaO), Augite range trends towards high Mg, low Al, Fe
	51.59		1A-19Q1	54-55	Characteristic high-Ca plagioclase (10-12% CaO), Augite range trends towards high Mg, low Al, Fe
	51.42		3A-22Y1	32-35	Characteristic high-Ca plagioclase (10-12% CaO), Augite range trends towards high Mg, low Al, Fe
					(Different composition observed in units between the prior sample and the next sample in core 3A)
	52.71		3A-22Y2	20-21	Characteristic high-Ca plagioclase (10-12% CaO), Augite range trends towards high Mg, low Al, Fe
	53.06		3A-22Y2B	53-58	Characteristic high-Ca plagioclase (10-12% CaO), Augite range trends towards high Mg, low Al, Fe
LB2 with hornblende (LB2-Hb)	52.98		1A-19Q2	85-92	Abundant HB, lower Na, K, Ti than IF, IID, or Ng'eju
	59.62		2A-25Y2	39-40	Abundant HB, lower Na, K, Ti than IF, IID, or Ng'eju
Tuff IIA??	53.36	*	3A-22Y2	85-89	Augite consistent with Tuff IIA or "Twiglet," insufficient grains of other minerals to confirm

(*continued on next page*)

Table 2 (*continued*)

Unit	MBS	Quality*	Core	Interval	Justification
Tuff IF	65.70	**	2A-28Y1	80-83	Feld, HB, Augite consistent with IF.
	65.89	**	2A-28Y2	10-12	Feld, HB, Augite consistent with IF.
	57.56	***	3A-24Y1	46-48	Feld, HB, Augite, Timag consistent with IF
	57.85	**	3A-24Y1	75-77	Feld, TiMag consistent with IF (surge).
Ng'eju	61.32	***	1A-22Q1	127-130	Aug, HB, Feld, Timag all consistent with Ng'eju (Ox most like Ng'eju upper)
	61.54	***	1A-22Q2	10-12	Aug, HB, Feld, Timag all consistent with Ng'eju
	61.90	***	1A-22Q2	46-48	Aug, HB, Feld, Timag all consistent with Ng'eju (Ox most like Ng'eju lower)
	69.62	**	2A-30Y1	59-65	Aug, HB, Feld consistent with Ng'eju. Few TiMag, more ilmenite
	69.93	**	2A-30Y1	93-95	Feld, Aug Ng'eju. HB abundant (some overlap with IF), Few TiMag preserved, but consistent with Ng'eju
	70.05	**	2A-30Y1	105-107	Feld, Aug Ng'eju. Few HB, TiMag analyzed, ilmenite abundant
	70.11	***	2A-30Y1	111-113	Feld, HB, Aug: Ng'eju. Abundant ilmenite
	60.43	*	3A-25Y1	33-35	Feld, Aug: mostly Ng'eju with some IE overlap. HB 100% Ng'eju.
Tuff IE	62.47	**	1A_22Q2	103-105	Consistent with IC/IE for feldspar, augite, TiMag and strat position break the tie.
	60.68	*	3A-25Y1	58-61	Feld: IE/IC, Augite: IE. No TiMag or HB
	61.42	***	3A-25Y1	132-134	Feld and Augite: IE/IC. Ox: IE/IC
	61.86	**	3A-25Y2	36.5-37.5	Feld: IE/IC. Augite: IE/IC and others (contaminated). Ox: IE
	62.10	***	3A-25Y2	61-63	Feld and Aug: IE/IC. Ox: IE
	62.68	*	3A-25Y2	119-121	Feld, Aug, and Ox: IE/IC. Abundant HB, unlike IE OR IC
	63.98	*	3A-26Y1	89-91	Feld, Aug, and Ox: IE/IC. Abundant HB, unlike IE OR IC
	64.25	**	3A-26Y1	117-119	Feld, Aug: IE/IC. No HB.
	64.94	***	3A-26Y2	36-42	Feld and Aug: IE/IC. Ox: IE
Tuff ID	62.62	**	1A-22Q2	118-120	Feldspar consistent with ID or Ng'eju, Augite and TiMag are ID.
	66.07	***	3A-26Y3	0-2	Feld, Aug, Ox consistent with ID
Tuff IC	65.04	**	1A-23Q2	62.5-63.5	Feld and aug consistent with IC/IE, TiMag breaks the tie
	71.95	**	3A-28Y2	137-138	Feld, Aug consistent with IC, no Ox
Tuff IB	65.60	**	1A-23Q2	119-121	Feld consistent with IF or IB, Aug and TiMag with IB
	71.97	**	2A-30Y3	11-13	Feld, Aug consistent with IB. Little/no TiMag preserved
	72.03	**	2A-31Y1	0-5	Feld, Aug consistent with IB. Little/no TiMag preserved
	72.48	**	3B-25Y1	61-62	Feld mostly IB (some scatter), but Augite and TiMag are completely consistent.
Below IB HB bearing	70.04		1A-25Q1	100-112	Feld mixed (plag, anclas), HB like Ng'eju, Aug like IC, TiMag mixed (overlaps IC/IE/Ng'eju)
	70.11		1A-25Q1	112-114	Feld mixed (plag, anclas), HB like Ng'eju, Aug like IC, TiMag not observed

(*continued on next page*)

Table 2 (*continued*)

Unit	MBS	Quality*	Core	Interval	Justification
CFCT	96.20	*	2A-39Y-1	20-25	Feld and augite mostly like CFCT (some mix). Oxides dominated by ilmenite.
	97.34	*	2A-39Y-2	133-135	Feld and augite like CFCT. Mix of ilmenite and titanomagnetite.
	97.65	**	2A-39Y2	23-24	Feld and augite like CFCT. Oxides like CFCT at Loc 71.
	98.15	*	2A-39Y-2	68-71	Feld and augite mostly like CFCT (Loc 9a, 1st Fault). Titanomagnetite and ilmenite mixed.
Naabi	104.65	**	2A-42Y2	124-126	Feldspar like Naabi, contains aenigmatite. Augite more mixed (some Naabi, some CFCT-like)
	106.23	**	2A-43Y1	126-128	Feldspar mostly Naabi (some more spread out, CFCT range). Augite Naabi, contains aenigmatite.
Orkeri	108.74	**	2A-44Y1	74-76	Feldspar, augite like Orkeri
	109.48	**	2A-44Y2	14-16	Feldspar, augite like Orkeri
	110.40	**	2A-44Y2	106-108	Feldspar, augite like Orkeri
Pre-Orkeri HB rich	110.48		2A-44Y2	114-116	Feld like Orkeri, but abundant HB rather than Augite
Pre-Orkeri mafic glass	178.04		2A-68Y-1	100-108	More mafic glass, feldspar like Naabi, ilmenite dominant.
Pre-Orkeri high-Fe aug	190.53		2A-72Y-2	11-13	Higher-Fe, lower-Mn augite
	190.66		2A-72Y-2	24-26	Higher-Fe, lower-Mn augite

main marker tuff of Upper Bed II), though its exposures in outcrop are intermittent since it is often cut out by a major disconformity (McHenry et al., 2016; McHenry and Stanistreet, 2018). Tuff IID is depositionally complex (with multiple units, including surge and airfall) and compositionally variable, but all units are characterized by abundant hornblende, which is compositionally unlike the (rare) hornblende of the underlying Bed II tuffs, especially in TiO_2. Tuff IID augite falls broadly into two distinct populations, one of which overlaps the Lower Bed II augite compositional range in most elements and the other characterized by higher Na and Mg. Individual samples of Tuff IID may contain both of these augite compositions, or favor one over the other. Feldspar is not diagnostic, as it covers a similar compositional range of anorthoclase into low-Ca plagioclase compared to Lower Bed II tuffs. Tuffs above IID within Bed II tend to have similar compositions; identifying this Tuff IID assemblage therefore does not fingerprint the specific tuff, but rather places it within a zone at or above the level of Tuff IID. The only sample from Bed II that yielded hornblende comparable to Tuff IID hornblende is in Core 3A at 46.06 mbs (Fig. 6b). This tuff also contains augite consistent with Tuff IID, though it lacks the distinctive high-Na and high-Mg population, and thus also overlaps in composition with tuffs from Lower Bed II (Fig. 6c). Feldspar and titanomagnetite were sparse in this sample. It should be noted, however, that this sample lies within the lower part of Bed II as reconstructed by Stanistreet et al. (2020), while Tuff IID is typically found near the top of Bed II in outcrop. No Tuff IID-composition hornblendes are observed in Cores 1A or 2A, suggesting that this interval was removed by a disconformity as is often observed for Tuff IID in outcrop.

5.1.2. High-Ca plagioclase-bearing tuff (HCPT)

Above the level of the Tuff IIA candidate in Core 3A, and also recognized in Core 1A, lies a new composition that has so far not been identified in outcrop. In feldspar (Fig. 5a), this composition consists of a tight compositional cluster of high Ca plagioclase feldspar (~10–12 wt % CaO) that is slightly less Ca-rich than the high-Ca plagioclase of the Bird Print Tuff (BPT) in outcrop (12.5–15 wt% CaO: McHenry et al., 2016; McHenry and Stanistreet, 2018). Its augite is also distinctive; while it overlaps in part with the broad compositional range exhibited by the BPT and Lower Bed II tuffs, most augite grains from all samples from this compositional group are distinctively higher in Mg and lower in Al, Mn, and Fe (Fig. 5b). This tuff composition will be referred to as the High-Ca plagioclase-bearing tuff (HCPT).

In Core 3A this HCPT composition is identified at 53.06, 52.71, and 51.42 mbs, each representing an individual single tuff within this zone. It should be noted that two other tuffs were sampled within that interval (at 52.46 and 52.51 mbs) are dominated by high-K anorthoclase rather than the intermediate-Ca plagioclase, though the tuff at 52.46 mbs does contain individual grains matching this new composition for both augite and feldspar. In Core 1A, this composition is recognized in a ~6 cm thick tuff at 51.52–51.59 mbs. This "pure" HCPT assemblage is not identified in Core 2A, though individual plagioclase and augite grains consistent with the HCPT composition are recognized (in an overall assemblage of anorthoclase and augite more consistent with Lower Bed II) in a sample at 61.11 mbs. This tuff is likely from the same stratigraphic interval as this new composition, perhaps equivalent to one of the "mixed" samples in Core 3A (e.g., the one at 52.46 mbs).

5.1.3. Lower Bed II tuff with hornblende (LB2-Hb)

A new, compositionally distinct tuffaceous sandstone (referred to as the Lower Bed II tuff with hornblende, or LB2-Hb) not previously identified in outcrop was recognized in Core 1A at 52.98 mbs and in Core 2A at 59.62 mbs. Its hornblende is abundant (which is unusual for a Bed II tuff below Tuff IID) and uniquely low in Na and Ti compared to both Tuff IID and Tuff IF (Fig. 6). Few anorthoclase feldspars were observed in the Core 2A sample and the Core 1A sample has a wide

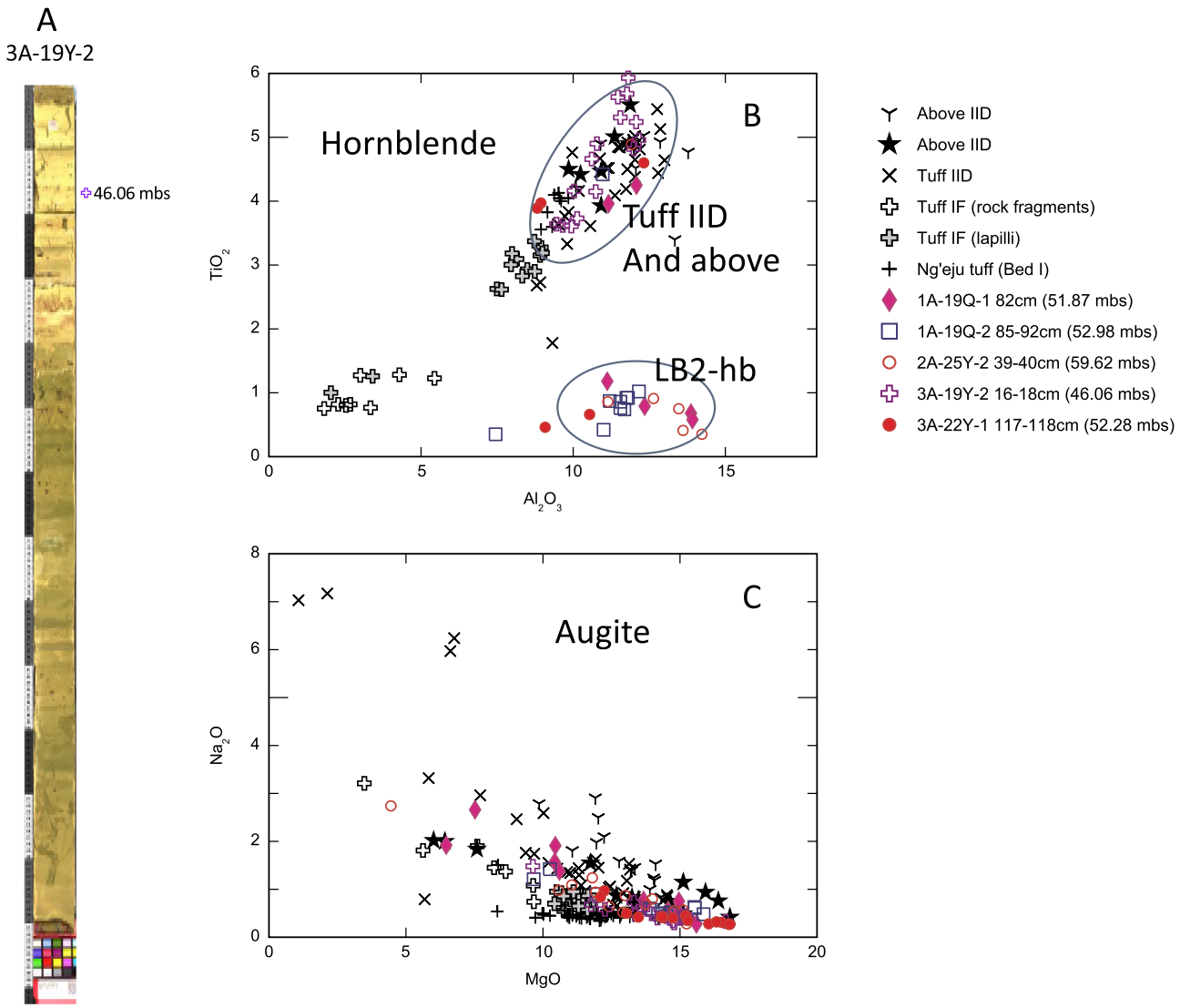

Fig. 6. Bed II hornblende-bearing tuffs (colored symbols) plotted against previously published Bed I and Bed II hornblende-bearing tuffs (black symbols). Blue circles highlight the range of composition of the main populations for select marker tuffs (note that some individual grains fall outside this range). A. Core image of core section 3A-19Y-2, with position of the sample at 16-18 cm (46.06 mbs) indicated. Positions of other samples are shown in Fig. 4. B. Hornblende compositions, TiO_2 vs. Al_2O_3. Sample 3A-19Y-2, 16–18 cm (46.06 mbs) plots with Tuff IID and above compositions, with higher Ti and Al than Lower Bed II or Bed I tuff hornblendes. A second population from core samples with lower TiO_2 hornblende (the Lower Bed II hb-bearing tuff, or LB2-hb) differs from outcrop samples, and can be identified in both cores 2A and 1A. C. Augite compositions, Na_2O vs. MgO. Only samples for which hornblende was also plotted are plotted here. The 46.06 mbs sample with Tuff IID-like hornblende does not overlap with the higher-Na population found in many outcrop Tuff IID samples, though it does overlap the lower-Na, higher-Mg range. (For interpretation of the references to color in this figure legend, the reader is referred to the web version of this article.)

range of compositions from anorthoclase to intermediate plagioclase, similar to many Lower Bed II tuffs, and its augite also covers a broad range but more closely resembles Lower Bed II compositions. Titanomagnetite is preserved in the Core 1A sample (at 52.98 mbs), and is generally high in MgO compared to other hornblende-bearing Bed II tuffs, and offset from Tuff IID titanomagnetite in its slightly lower Al_2O_3 compared to MgO (with some overlap: see Fig. 6).

5.1.4. Tuff IIA

Tuff IIA has not been confirmed in any of the cores, although a ~3 cm thick reworked tuff at 53.36 mbs in Core 3A cannot be ruled out. While titanomagnetite was not preserved, feldspar was sparse (only 4 grains analyzed, covering a range of compositions), and abundant detrital quartz and calcite was observed, its augite composition appears to be consistent with Lower Bed II tuffs (most similar to Tuff IIA, though also overlapping the "Twiglet" unit: McHenry et al., 2016; McHenry and Stanistreet, 2018) across all elements analyzed. In particular, FeO, MgO, MnO, and Na_2O values separate this composition from Upper Bed II tuffs (e.g. Tuff IID, see Fig. 5), and its lack of hornblende and high-Ca plagioclase separate it from other lower to middle Bed II tuffs analyzed in this study. This, in combination with its stratigraphic position and association with chert nodular horizons in the core that are characteristic of the Tuff IIA level in outcrop, lead us to provisionally correlate this tuff with Tuff IIA.

5.2. Bed I tuffs

Olduvai Bed I tuffs tend to be thicker, more continuous, and less contaminated than their Bed II counterparts in outcrop (e.g. Hay, 1976; McHenry et al., 2016), and the same is seen in all of the cores. The cores often show multiple eruptive or depositional units separated by lacustrine sediments, indicating that the "tuffs" were usually not derived from single, but multiple eruptive events. In outcrops outside of the lake basin, these primary and reworked volcanic units may appear to be less

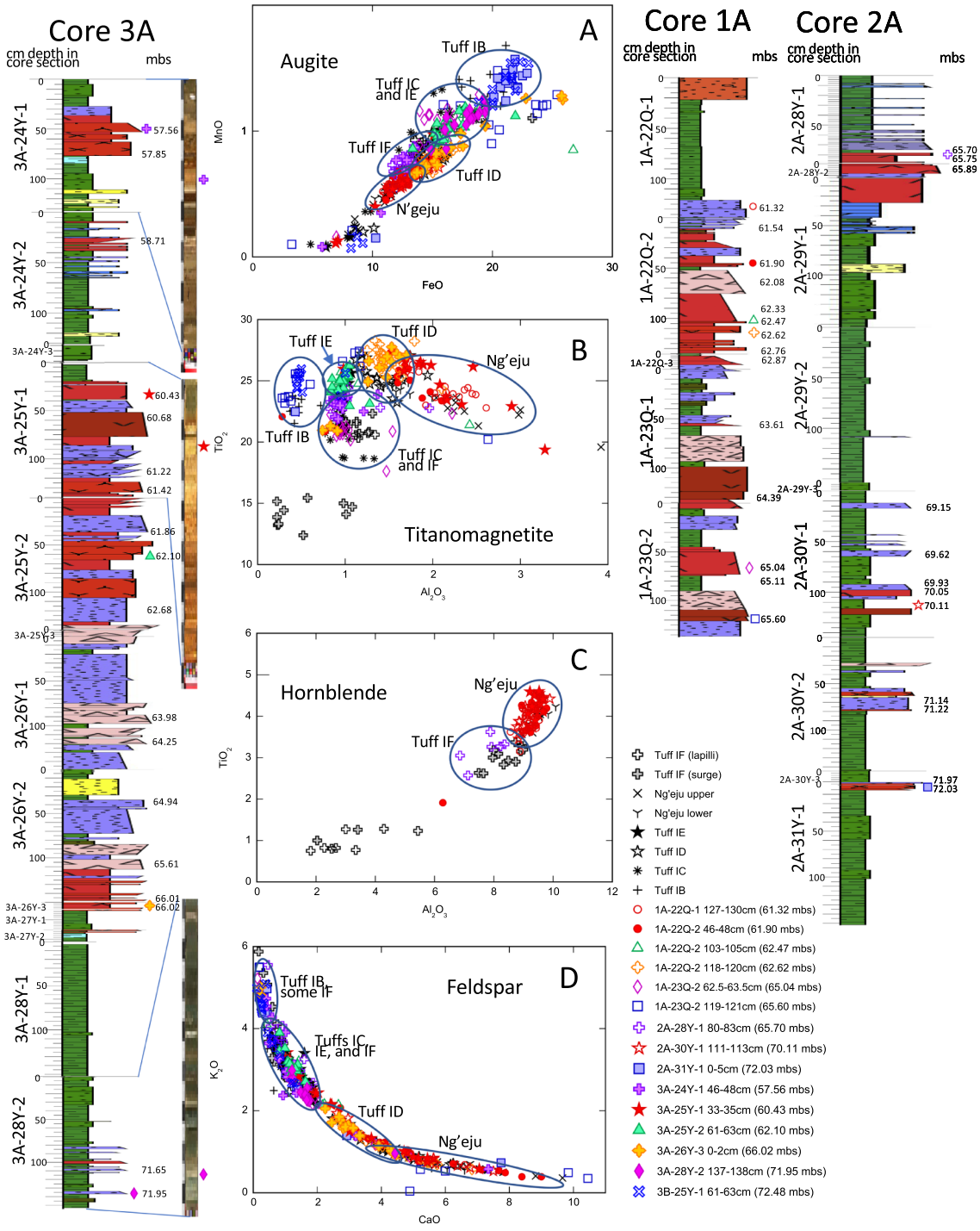

Fig. 7. Upper Bed I core sections, with example core segment photos, positions of all samples, and mineral composition plots. Key for colors (indicative of facies) in Fig. 3. Selected samples are plotted against published geochemical "type" samples (black symbols) for Bed I tuffs from McHenry (2005, 2012). Blue circles highlight the range of composition of the main populations for select marker tuffs (note that some individual grains fall outside this range). A. Augite compositions, MnO vs. FeO. Samples can be separated into ranges that overlap Bed I marker tuffs from outcrop, including Tuff IB, Tuff ID, Tuff IF, and Ng'eju, with some overlap. Tuffs IC and IE are indistinguishable in augite. B. Titanomagnetite compositions (for all samples preserving titanomagnetite), TiO_2 vs. Al_2O_3. Tuffs IB, ID, IE, and Ng'eju plot separately, while Tuffs IC and IF overlap. The lower TiO_2 concentration in Tuff IC titanomagnetite compared to Tuff IE is one of the only ways to distinguish between the two tuffs using major elements. C. Hornblende, TiO_2 vs. Al_2O_3. Hornblende is rare in Bed I, largely limited to Tuffs IF and Ng'eju, which plot separately. D. Feldspar compositions, K_2O vs. CaO. Tuff IB has high-K anorthoclase (with some overlap from a minor population from Tuff IF), Tuffs IC, IE, and most of IF have intermediate anorthoclase, and Tuff ID and the Ng'eju Tuff have plagioclase (trending towards higher CaO for Ng'eju). (For interpretation of the references to color in this figure legend, the reader is referred to the web version of this article.)

discrete, without intervening lacustrine sediments and with less overall accommodation space. To address this, McHenry et al. (2013) employed a geochemical "zone" approach to Bed I tuff fingerprinting in lake margin sediments, in which multiple different samples (from different, but typically consecutive) units recognized in the core are considered to be part of the Tuff IE "zone" or the Ng'eju Tuff "zone." This approach is also used here. While not all of the major, already named tuffs (Tuffs IB, IC, ID, IE, Ng'eju, and Tuff IF) are present in every

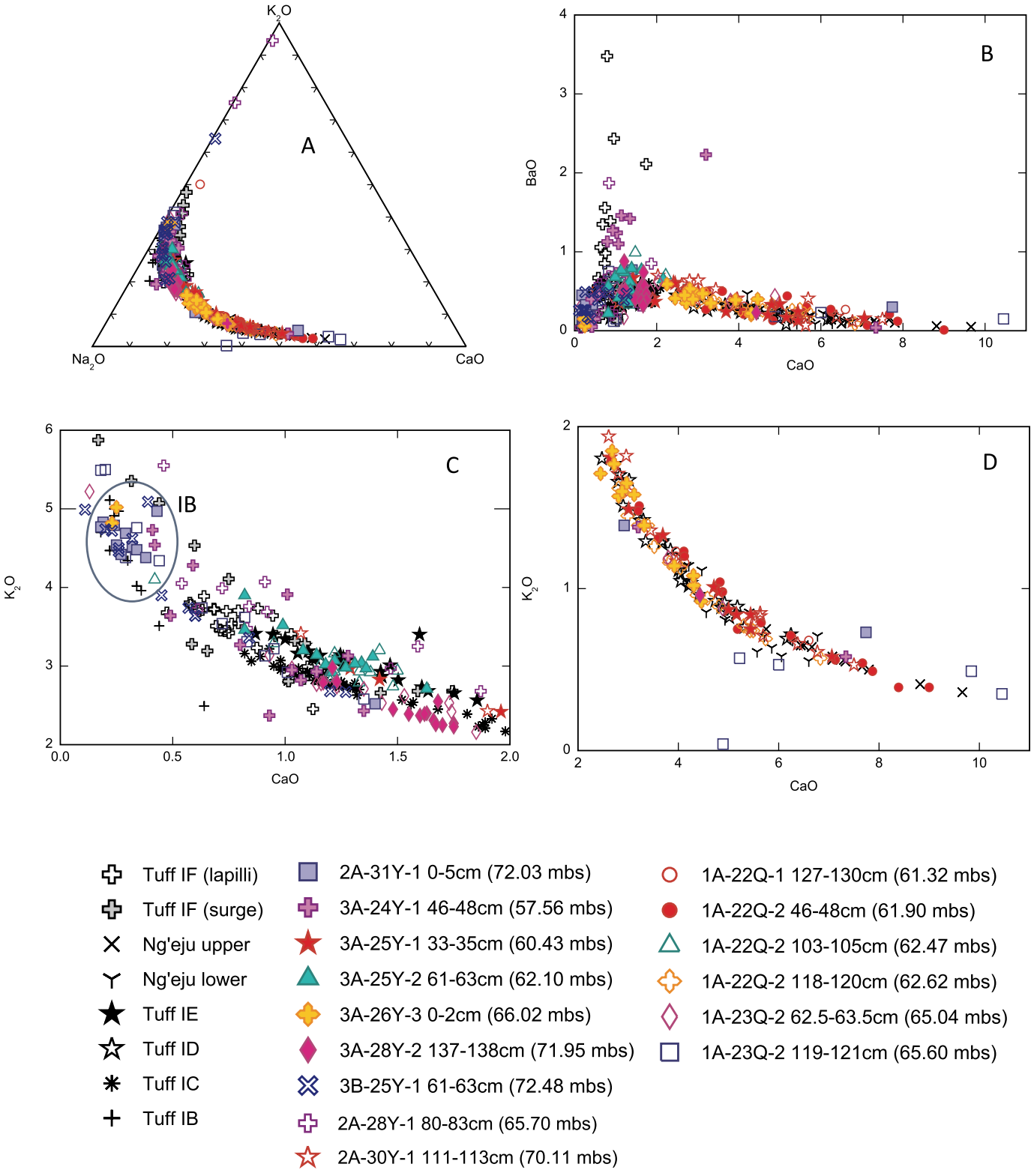

Fig. 8. Upper Bed I feldspar compositions. Same symbols, and same stratigraphic positions of samples indicated in Fig. 7. A. Feldspar ternary diagram. B. Feldspar composition, BaO vs. CaO. Tuff IF has a population of distinctively high Ba anorthoclase. C. Anorthoclase composition, K_2O vs. CaO (plot shows samples with CaO concentrations up to 2 wt% and K_2O concentrations up to 6 wt% only). This shows the high-K anorthoclase concentration of Tuff IB (the main population is highlighted in the blue circle), and the overlap between Tuffs IC, IE, and IF. D. Plagioclase composition, K_2O vs Cao (CaO concentrations over 2 wt% only). This shows Tuff ID with higher K_2O and lower CaO, overlapping with Ng'eju, which trends towards higher CaO. (For interpretation of the references to color in this figure legend, the reader is referred to the web version of this article.)

core, all are identified in at least one of the three cores, based upon a combination of mineral assemblage, phenocryst composition, and relative stratigraphic position. Since there were too many samples collected in the Upper Bed I interval to be plotted together in a readable diagram, selected samples from each interval are plotted in Fig. 7 to show these general correlations. The positions of all collected samples are shown on the stratigraphic figures, and data for all samples analyzed are presented in the appendices.

5.2.1. Tuff IF

Tuff IF can often be identified in outcrop based on its distinctive layered appearance, with pyroclastic surge deposits interlayered with lapilli-rich airfall units (Stollhofen et al., 2008; Stollhofen and Stanistreet, 2012). Mineralogically and geochemically it is characterized by its K and Ba-rich anorthoclase feldspar (Fig. 8) and its abundant hornblende content (unlike other anorthoclase-bearing Bed I tuffs: McHenry, 2005, 2012), shown in Fig. 7. Its characteristic layered appearance was immediately recognized in cores 2A and 3A, as they were initially split, because of the obvious similarity to the appearance of Tuff IF at RHC (Locality 80). That identification was confirmed based upon the mineral assemblages and phenocryst compositions observed in multiple samples (65.70 and 65.89 mbs in core 2A; 57.56 and 57.85 mbs in core 3A). Tuff IF appears to be absent in core 1A, where an unconformity, identified as the Crocodile Valley Incision Surface (CVIS) by Stanistreet et al. (2020), separates Ng'eju-composition tuffs from younger Bed II sediments.

5.2.2. Ng'eju tuff

The Ng'eju Tuff, first described in detail by McHenry (2005, 2012), is characterized by plagioclase feldspar and hornblende, an assemblage that separates it from other Bed I tuffs, along with augite and titanomagnetite. Within the cores, Ng'eju composition is recognized at appropriate stratigraphic levels in all three cores, though multiple units within this interval (between Tuffs IE and IF) share it. Subtle compositional differences between Upper and Lower Ng'eju previously identified from outcrop samples (e.g., more Ca-rich plagioclase and lower Fe and Mg augite in the upper unit: McHenry, 2012) are also observed in Core 1A, where the uppermost sample (at 61.32 mbs) resembles the Upper Ng'eju from outcrop, while the lowermost sample (at 61.90 mbs) resembles the Lower Ng'eju composition (Figs. 7, 8).

5.2.3. Tuff IE

In outcrop, Tuff IE is represented as a pyroclastic flow on the First Fault (at Locality 1, north of the gorge) as dominantly pyroclastic flows and airfall tuffs in the eastern basin (e.g., Locality 6), and as dominantly surges and airfall tuffs in the Junction Area (where the Main and Side Gorges meet, Hay, 1976; Stollhofen and Stanistreet, 2012) and western gorge. Its mineral assemblage includes lower-K anorthoclase (compared to Tuff IF and IB), augite, and titanomagnetite, and where preserved its glass is trachytic. Its composition is so similar to Tuff IC that the two cannot be distinguished using major element feldspar, glass, and augite compositions, though differences in titanomagnetite composition (particularly in TiO_2) can help distinguish them (McHenry, 2005, 2012). Using this approach, Tuff IE compositions are identified (see Fig. 7) in eight samples from Core 3A between Tuff ID and the Ng'eju Tuff (from 60.68 to 64.95 mbs) and in one sample from Core 1A (at 62.47 mbs). Two of the samples within the Tuff IE zone in Core 3A (at 62.68 and 63.98 mbs), while they are consistent with IE in terms of augite, feldspar, and titanomagnetite, also contain abundant hornblende, which is not observed in outcrop for Tuff IE. Titanomagnetite was not preserved in this interval from Core 2A making it impossible to confirm Tuff IE vs. IC, though samples at 71.14 and 71.22 mbs could be either IC or IE based upon the rest of the assemblage. Since Tuff ID is also missing in Core 2A (see section below), stratigraphic position relative to this more distinctive unit is not possible.

5.2.4. Tuff ID

In outcrop, Tuff ID is one of the more distinctive tuffs in Bed I, with its abundant plagioclase feldspar, salt-and-pepper appearance (with abundant augite), and lack of hornblende. Its augite and titanomagnetite is distinct from other Bed I tuffs in multiple elements (McHenry, 2005, 2012). This tuff is recognized in Core 1A at 62.62 mbs and in Core 3A at 66.02 mbs, and is not observed in Core 2A (Fig. 7).

5.2.5. Tuff IC

Tuff IC is a marker tuff of local interest in the Olduvai Junction Area, where it directly overlies the *Zinjanthropus* paleoanthropological site and *Zinjanthropus* palaeolandscape surface (Blumenschine et al., 2012). It can be identified in the Western Gorge (based on its composition and position relative to the more distinctive Tuffs IB and ID), but not in the Eastern Gorge or First Fault areas. It is mineralogically similar to Tuff IE, with indistinguishable augite, feldspar, and glass compositions (McHenry, 2005, 2012), though its titanomagnetite (where preserved) is less Ti-rich. Within the cores, Tuff IC can only be confirmed compositionally in Core 1A (at 65.04 mbs) where its titanomagnetite serves to distinguish it from IE (Fig. 7). It can be inferred for Core 3A (at 71.95 mbs), where a sample matching IC or IE in feldspar and augite (but lacking the titanomagnetite needed to compositionally distinguish between the two) is found stratigraphically below the level of Tuff ID.

5.2.6. Tuff IB

Tuff IB is a major marker in Bed I, appearing as a succession of pyroclastic flow and airfall deposits in the Eastern Gorge, dominantly airfall tuffs in the Junction Area and the lake (e.g. Locality 80), and as mostly reworked tuff in the Western Gorge (McHenry, 2005, 2012; Habermann et al., 2016). It is often associated with dark pumice, and fallout tuff units often have a feldspar crystal-rich base. Mineralogically it is characterized by distinctive low-Ca and Ba anorthoclase, high-Fe and Mn augite, and low-Al titanomagnetite (Fig. 7). In the OGCP cores this assemblage is recognized in Cores 2A (at 71.97 and 72.03 mbs), 1A (at 65.60 mbs), and 3B (at 72.48 mbs). Since Core 3A and 3B were obtained at the same site, its position in Core 3B can be used to approximate its position in Core 3A, based on overall similarities between the two.

5.3. Ngorongoro Formation (pre-Bed I basalt lava)

Stanistreet et al. (2020) describe a new Formation (the Ngorongoro Formation) which includes the thick, volcanically-sourced units found in the OGCP cores below the level of the Bed I basalt lava. This includes some volcaniclastic units previously described from outcrop (Coarse Feldspar Crystal Tuff (CFCT), Naabi Ignimbrite, and Orkeri Ignimbrite), plus many additional units below. The upper part of this Formation is present in both Cores 2A and 3A, although the full extent, including two major pulses of Ngorongoro-derived volcaniclastic material separated by lacustrine deposits, is observed only in Core 2A. The three main ignimbrites previously known from the First Fault Orkeri exposures (McHenry et al., 2008; Habermann et al., 2016) can all be compositionally identified in Core 2A. Those below this level are not known from outcrop.

Because of the large number of samples collected from the cores in this lower interval, samples plotted in the following figures are separated into the upper interval (overlapping with the outcrop record, including likely correlates for the CFCT, Naabi, and Orkeri) and lower interval (below 120 mbs in Cores 2A and 3A). Fig. 9 shows the stratigraphic position of the samples collected for the upper interval. It should be noted that sample analysis for the lowest part of Core 3A is still underway, thus only the 2A core has been systematically analyzed as part of the current study.

5.3.1. Coarse Feldspar Crystal Tuff

The Coarse Feldspar Crystal Tuff (CFCT) is a marker unit above the

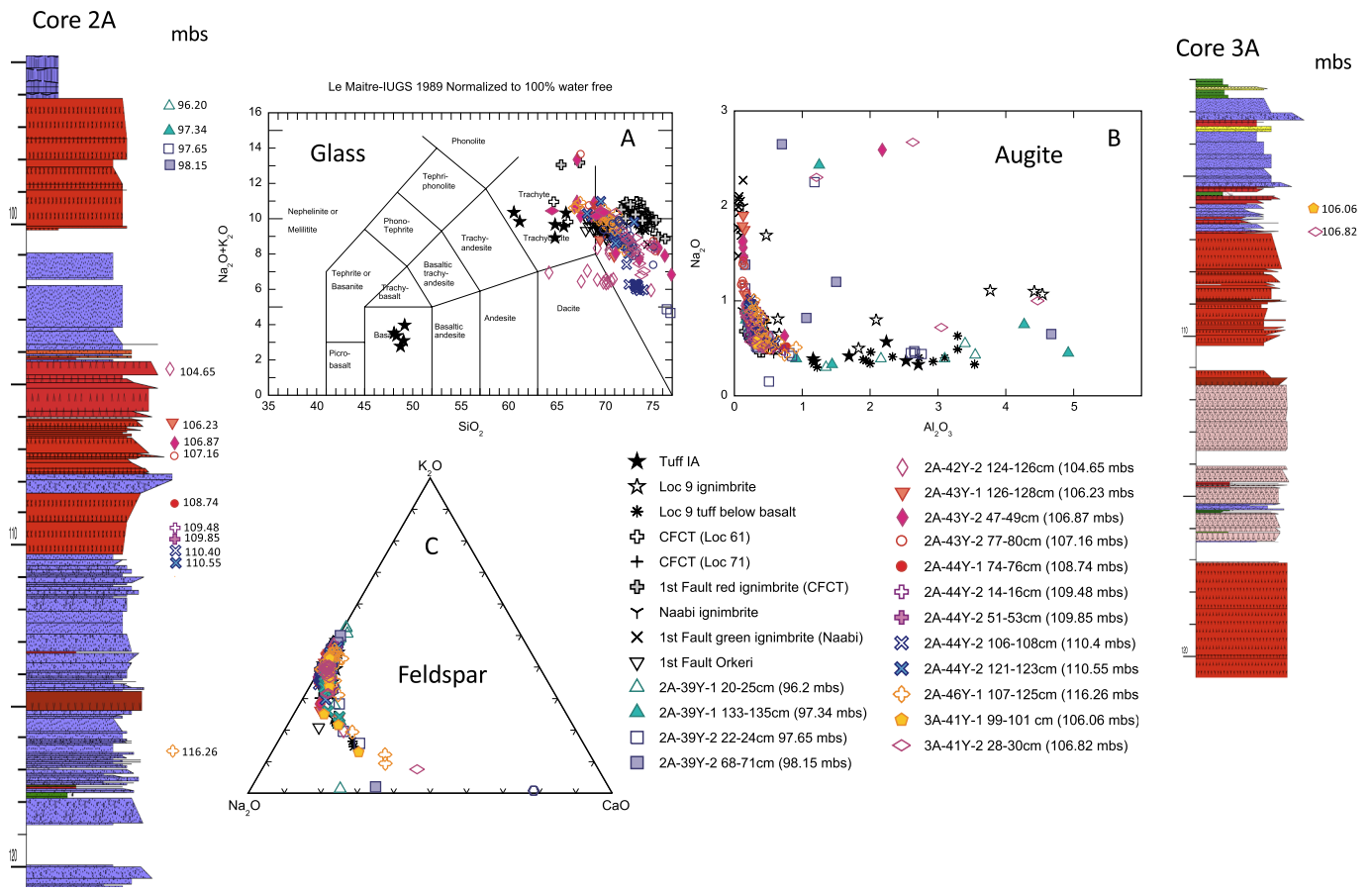

Fig. 9. Stratigraphic sections for the upper part of the Ngorongoro Formation, Cores 2A and 3A, down to 120 mbs, sample positions, and glass and mineral plots. Key for colors (indicative of facies) in Fig. 3. Plots include (dark symbols) "type" section compositions for Lower Bed I marker beds or other outcrop samples from McHenry et al. (2008), McHenry (2012), and Habermann et al. (2016). Position of all samples analyzed indicated. A. Glass compositions, for samples containing minimally-altered glass. Total alkali vs. silica (TAS) diagram after Le Maitre et al. (1989). Most glass plots as rhyolite, though some shards trend towards trachyte. B. Augite composition, Na_2O vs. Al_2O_3, showing full range of high-Al population. This high-Al composition is recognized in outcrop at Locality 9a, and also in Core 2A at 96.20 and 97.65 mbs. Likely Naabi equivalents have higher Na_2O augites. C. Feldspar ternary diagrams, showing that most samples contain only anorthoclase.

Naabi Ignimbrite in the western gorge, that has also been correlated to a red ignimbrite on the First Fault scarp (Orkeri outcrop) above the green ignimbrite associated with the Naabi (McHenry et al., 2008; Habermann et al., 2016). In the Western Gorge at Locality 61, a grey ash associated with this unit yielded an assemblage of augite, hornblende, titanomagnetite, ilmenite, anorthoclase (less K-rich than Naabi, and with lower FeO), and rhyolitic glass (McHenry, 2012). At Locality 71, a coarser part of the CFCT has a slightly different assemblage, lacking hornblende. Samples of both, and of the First Fault ignimbrite, are plotted against samples from the core to see if units from the core are geochemically and mineralogically consistent with any of the previously described CFCT outcrop samples. While multiple samples collected between the Naabi and the Bed I basalt in Core 2A register CFCT compositions in one or more minerals (forming a "CFCT zone", Fig. 9), the most consistent sample overall is from 97.65 mbs (an orange lapilli ash tuff). The feldspars (Fig. 10) and augites overlap well with CFCT data from outcrop equivalents (Fig. 11), though this cannot be confirmed with glass (since there were only 2 grains analyzed).

Mineralogical differences between the four samples collected within this CFCT "zone" in Core 2A may help explain differences observed between different CFCT samples collected from outcrop, and help confirm that the ignimbrite exposed under the Bed I basalts at Locality 9a (previously rejected as a CFCT correlate based primarily on its population of high-Fe augite and the dominance of ilmenite over titanomagnetite: McHenry et al., 2008; McHenry, 2012) could fit within this zone. The Locality 9a ignimbrite, which was only sampled at its top due to limited exposure at the base of the gorge, has the same high-Al, high-Ti augite population observed in sample 2A-39Y-1 20–25 cm, at 96.2 mbs, the uppermost sample collected from this unit within the core. The Loc 9a ignimbrite sample also contains abundant ilmenite rather than titanomagnetite, again similar to this core sample. The three lower samples (at 97.34, 97.65, and 98.15 mbs) contain some of this unusual augite composition (with more augite typical of previous CFCT samples), and while ilmenite is observed in all four, titanomagnetite dominates in the lower three. It is thus likely that the CFCT zone is compositionally zoned, with ilmenite more abundant at its top and titanomagnetite near its base, and that the ignimbrite exposure at Loc 9a corresponds to the top unit.

5.3.2. *Naabi Ignimbrite*

The Naabi Ignimbrite is the oldest unit in outcrop in the Olduvai Basin, where it sits directly above Precambrian basement rock in the Western Gorge. Within OGCP core 2A, it appears to sit at about 105 m below the surface (mbs), which is about the mid-point of this core. Compositionally, the Naabi can be recognized based on several unusual mineralogical or geochemical features: first, the presence of the mineral aenigmatite (so far not recognized in other units at Olduvai), high-K anorthoclase feldspar that is also slightly higher in FeO than other feldspar from Olduvai, and glass (where present) that is characteristically low in Al_2O_3. These "fingerprints" are described in McHenry et al. (2008), where they are used to correlate between the Naabi ignimbrite exposed in the Western Gorge and the green ignimbrite

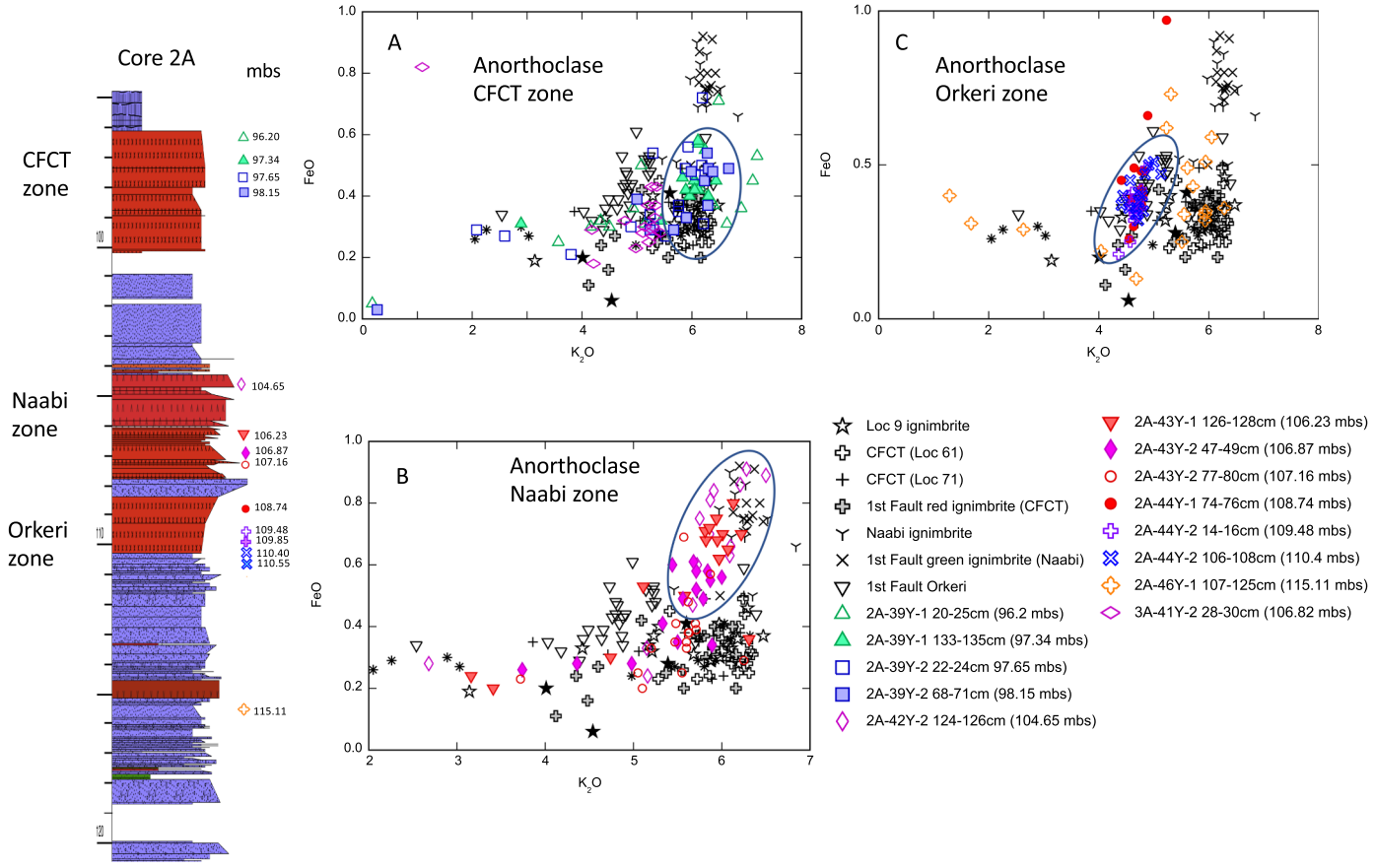

Fig. 10. Anorthoclase compositions for the upper part of the Ngorongoro Formation, Cores 2A and 3A, down to 120 mbs. Plots against previously published outcrop data (same as in Fig. 8), with core samples separated by zone. Key for colors (indicative of facies) in Fig. 3. A. Coarse Feldspar Crystal Tuff (CFCT) zone anorthoclase, FeO vs. K_2O. B. Naabi zone anorthoclase, FeO vs. K_2O. Naabi anorthoclase trends towards higher FeO concentrations. C. Orkeri zone anorthoclase, FeO vs. K_2O. Orkeri anorthoclase if offset from CFCT, with lower K_2O.

exposed along the First Fault (Orkeri outcrop, further described in Habermann et al., 2016). This composition occurs in two analyzed samples for Core 2A (at 104.65 and 106.23 mbs); both contain aenigmatite and high-K anorthoclase with elevated FeO (Fig. 10). While both samples contain glass, this appears to be heavily leached, with unusually low concentrations of both K_2O and Na_2O (both elements are susceptible to leaching, and to volatile loss during EPMA analysis). While less diagnostic, the augite composition of both samples is also consistent with Naabi, especially in its low Al_2O_3 (Fig. 11). In Core 3A, aenigmatite is identified in a sample at 106.87 mbs, but the other minerals appear to be a mixture of different compositions, suggesting a reworked deposit incorporating clasts from multiple units (including some Naabi-composition glass).

5.3.3. *Orkeri ignimbrite*

The Orkeri ignimbrite, first described by Habermann et al. (2016), lies below the Naabi-equivalent ignimbrite along the First Fault. No outcrop of this ignimbrite is exposed in the Olduvai Basin. It can be distinguished from the overlying Naabi and CFCT ignimbrites based on its lower-Fe and higher-Na augite (Fig. 11) and its higher-Ba, lower-K anorthoclase feldspar (Fig. 10). This composition is observed in three samples from Core 2A, at 108.74, 109.48, and 110.4 mbs.

5.4. *Tuff compositions below the Orkeri*

Below the Orkeri ignimbrite, the cores expose multiple ignimbrites and other volcanic or volcaniclastic units that have no known outcrop analogs for comparison. Most contain rhyolitic glass, while some (such as the lava at the base of Core 3B, at 142.38 mbs) are trachytic (Fig. 12). This Core 3B sample (142.38 mbs) is also an outlier in Al_2O_3 (high) and FeO (low) for its glass (Fig. 13). This high Al_2O_3 is unusual for a glass and suggests a potential analytical overlap with feldspar microlites, however all shards analyzed for this sample were frothy glass with no visible microlites using BSE, and the shards have very consistent compositions. If the influence of microlites below the surface were responsible for high Al_2O_3, larger differences in Al_2O_3 concentrations between different shards would be expected. A sample at 178.04 mbs in Core 2A has some glass shards consistent with more mafic glass compositions (Figs. 12 and 13). Feldspar in the lower part of the cores is dominantly anorthoclase, with few grains of plagioclase for many samples (Fig. 12). The sample at 178.04 mbs in Core 2A (with the mafic glass) also has higher Fe-anorthoclase than others in this stratigraphic range (Fig. 13). Augite covers a broad compositional range from Mg-rich to Mg-poor, with certain units plotting in very tight compositional ranges that could potentially help fingerprint them, e.g. distinctively high FeO in samples around 190.53 mbs in Core 2A, and a dispersed, high-MgO population in the deepest sample analyzed at 202.6 mbs in Core 2A (Figs. 12, 13).

6. Discussion

Fig. 5 shows the proposed tephra correlations between the three cores and a composite outcrop section, with the major tuffs indicated. Many tuffs recognized in outcrop do not appear to have equivalents in any of the cores.

While the Bed I tuff record from the OGCP cores match the outcrop record well (with all major marker beds identified in at least one core, and some marker beds identified in all cores), the correspondence

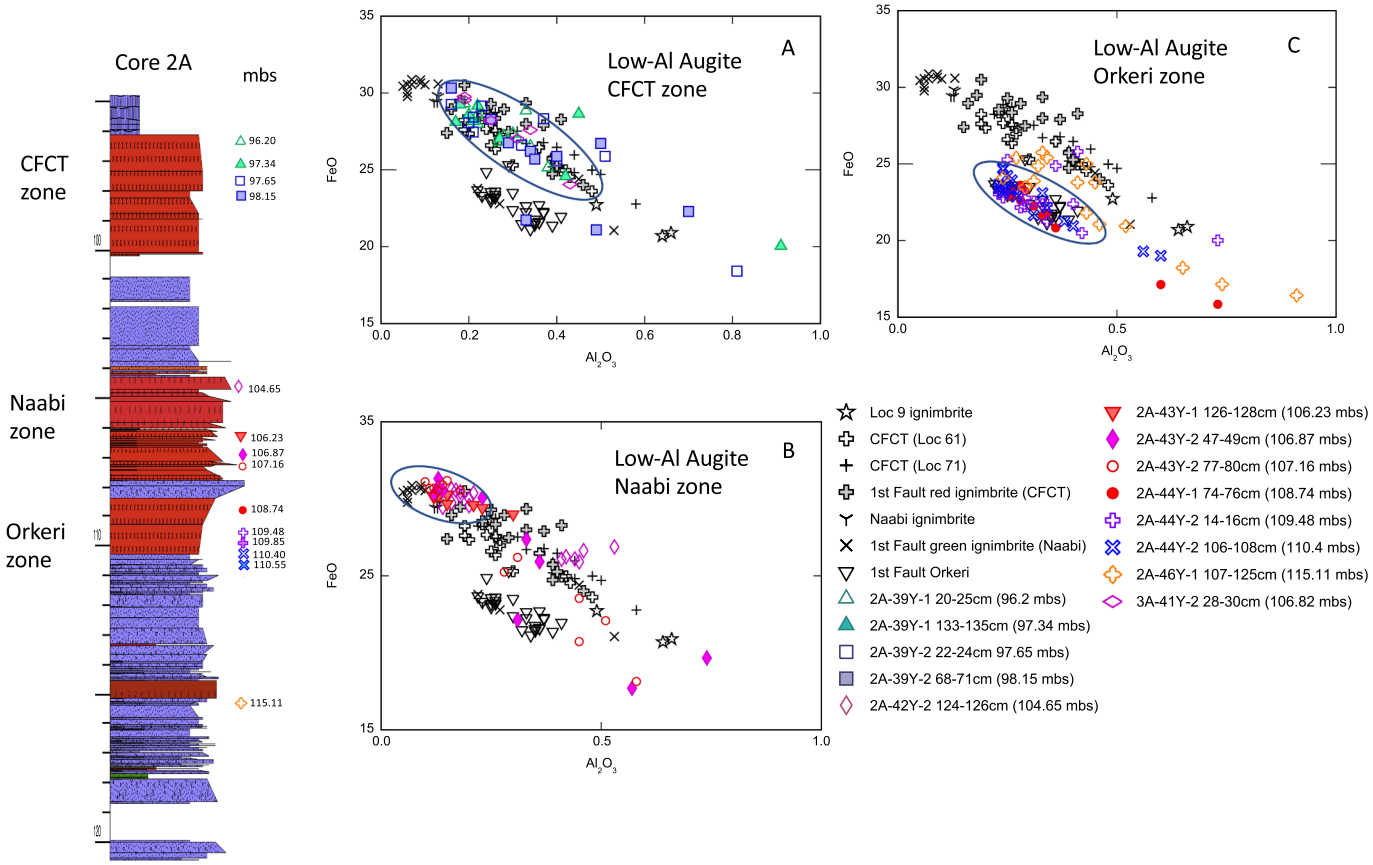

Fig. 11. Low-Al augite (up to 1 wt% Al_2O_3 only) compositions for the upper part of the Ngorongoro Formation, Cores 2A and 3A, down to 120 mbs. Key for colors (indicative of facies) in Fig. 3. The full range of augite compositions (including high-Al augite) is presented in Fig. 9. Plots against previously published outcrop data (black symbols, same as in Fig. 8), with core samples (colored symbols) separated by zone. A. Coarse Feldspar Crystal Tuff (CFCT) zone augite, FeO vs. Al_2O_3. B. Naabi zone augite, FeO vs. Al_2O_3. Naabi augite trends towards higher FeO concentrations compared to CFCT or Orkeri. C. Orkeri zone augite, FeO vs. Al_2O_3. Orkeri augite are offset from CFCT, with lower FeO.

between the cores and Bed II was disappointing. None of the major Bed II marker tuffs were definitively identified. This can be attributed to several factors, first, that the Bed II tuffs are more difficult to fingerprint even in outcrop, due to overlapping compositions, more pronounced reworking and mixing with non-juvenile material, and their less continuous preservation. As a result several potential correlations between the core and outcrop in Bed II cannot be ruled out (e.g., potential correlates for Tuffs IID and IIA based on one or two minerals that don't constitute unique fingerprints). Many Bed II stratigraphic exposures also lack tuffs due to erosion and uneven deposition, as discussed in McHenry et al. (2016). Tuff IID, one of the thickest and most recognizable marker beds within Bed II, is often cut out by a major incision, and it is therefore not surprising (though unfortunate) that none of the cores happened to penetrate parts of the Olduvai record where it is preserved. Second, in all three cores most of Bed II is lacustrine, while the best preserved examples of the Bed II tuffs in outcrop are from lake margin or subaerial areas. Tuffs in the lake are both thinner and more altered by interaction with saline-alkaline waters, which limits the preservation of glass and titanomagnetite. Tuff samples from Bed II were also more likely to be contaminated by quartz and/or calcite, indicating some mixing of volcaniclastic material with non-juvenile components, e.g. by turbidity currents, tempestites and/or wave reworking. Coarse calcite crystals form authigenically within the lake sediments (e.g. Hay and Kyser, 2001), and would thus be locally available for incorporation. Note that such mixing would be less obvious in the Eastern Gorge in the lake margin area, where other sediment would be sourced from Ngorongoro volcanics rather than from lake sediments and quartz-bearing Precambrian basement.

While no tuffs from outcrop are unambiguously identified in the cores for Bed II, a new tuff (designated the high calcium plagioclase tuff (HCPT)) has been identified in two of the cores, with a likely equivalent in the third. This tuff is similar in its mineral assemblage to the Bird Print Tuff (BPT) identified in outcrop, but its plagioclase is slightly less rich in CaO. Further sampling of this interval in outcrop will be required to tie it in precisely, though it is assumed to be in a similar stratigraphic position to the BPT. However, it does serve as a way to directly correlate between Cores 1A and 3A. Another new tuff (designated the Lower Bed II tuff with hornblende (LB2-Hb)) is also identified in the Cores 1A and 2A. It contains hornblende (unusual for Bed II) and is compositionally distinct in other minerals as well. Again, detailed sampling of thinner units in outcrop at Olduvai in the Tuff IIA and IIB range may yield outcrop correlates.

The Bed I tuffs are also mostly preserved within lacustrine intervals in the cores, which again limits the preservation potential of glass and titanomagnetite. However, the Bed I tuffs are thicker, better preserved, and less detritally contaminated overall. In some cases, multiple units (in some cases separated by lacustrine claystones) can have the same mineral assemblage and mineral compositions, constituting a “zone” rather than an individual airfall tuff. The Ng'eju (in Cores 1A and 2A) and Tuff IE (in core 3A) intervals in particular are often represented by multiple samples from stratigraphically distinct units. This is consistent with outcrop observations. For example, a stratigraphically separated lower “vitric” and an upper “ignimbrite” unit of Tuff IE are reported in the Eastern Gorge (McHenry, 2012), and multiple units of Ng'eju lapilli were observed at Locality 13 (DK) at the base of the Bed II section reported in Stanistreet et al. (2018). McHenry et al. (2013) used this

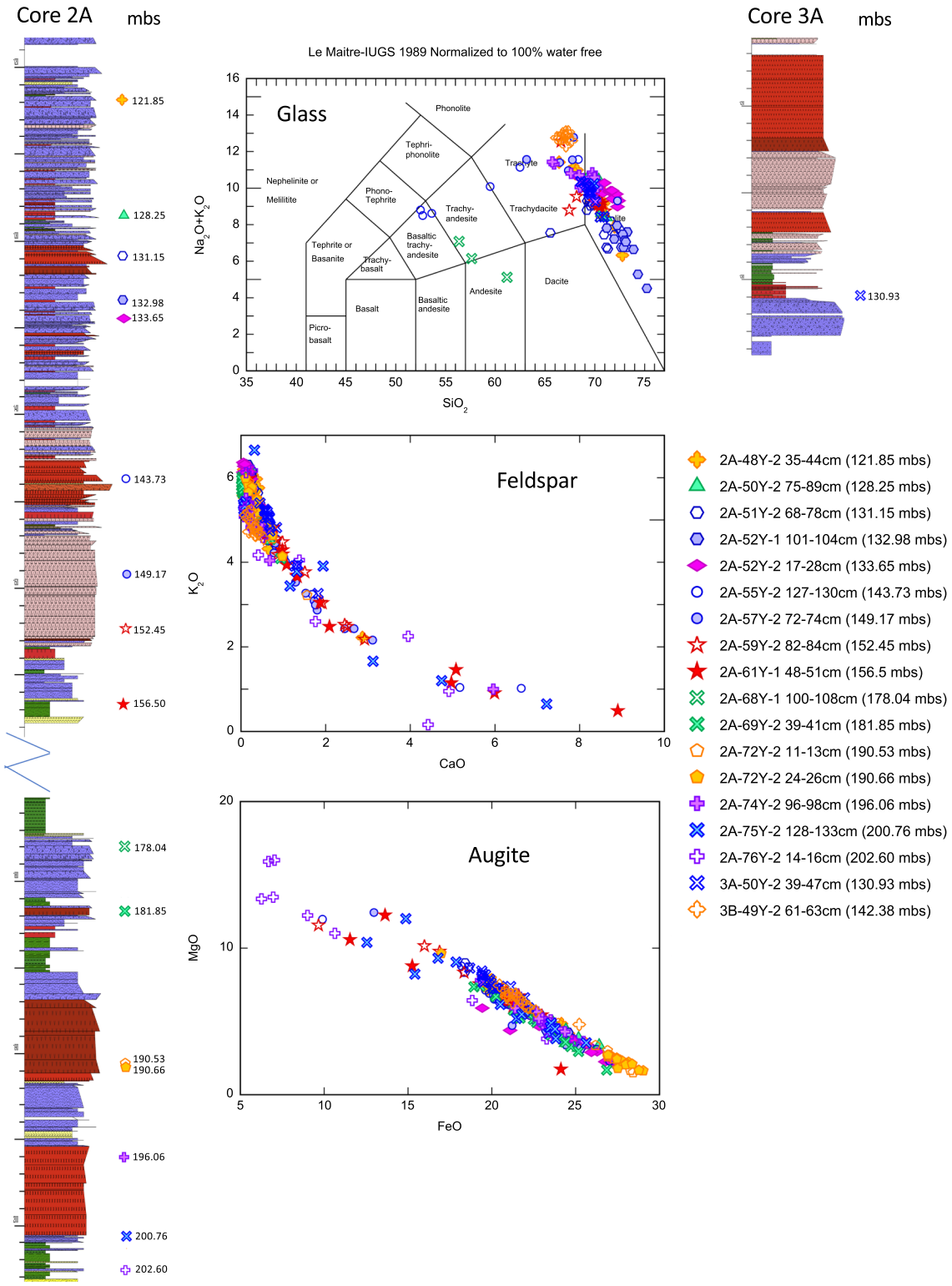

Fig. 12. Stratigraphy and compositional plots for the lower part of the Ngorongoro Formation, Cores 2A and 3A, below 120 mbs. Key for colors (indicative of facies) in Fig. 3. Note the break in the stratigraphic column between 158 and 175 mbs in Core 2A, where a lacustrine interval of the interfingering Naibor Soit Formation interrupts the volcaniclastic record. Sample positions are indicated on the column, along with the symbol used for each on the data plots. A. Lower Ngorongoro Formation glass compositions, Total alkali vs. silica (TAS) diagram. Most samples with glass were rhyolites, with the exception of the trachyte at the base of Core 3B and the trachyandesite in Core 2A at 178.04 mbs. B. Lower Ngorongoro Formation feldspar compositions, K_2O vs. CaO. Most volcaniclastic units in this interval have anorthoclase feldspar, with plagioclase present as a minor population in a few samples. C. Lower Ngorongoro Formation augite compositions, MgO vs. FeO. Certain intervals have distinctive augite: at 190.53–190.66 mbs in Core 2A, augite is distinctively high in FeO and low in MgO, and the deepest sample from the core at 202.6 mbs has a range of high-Mg augites.

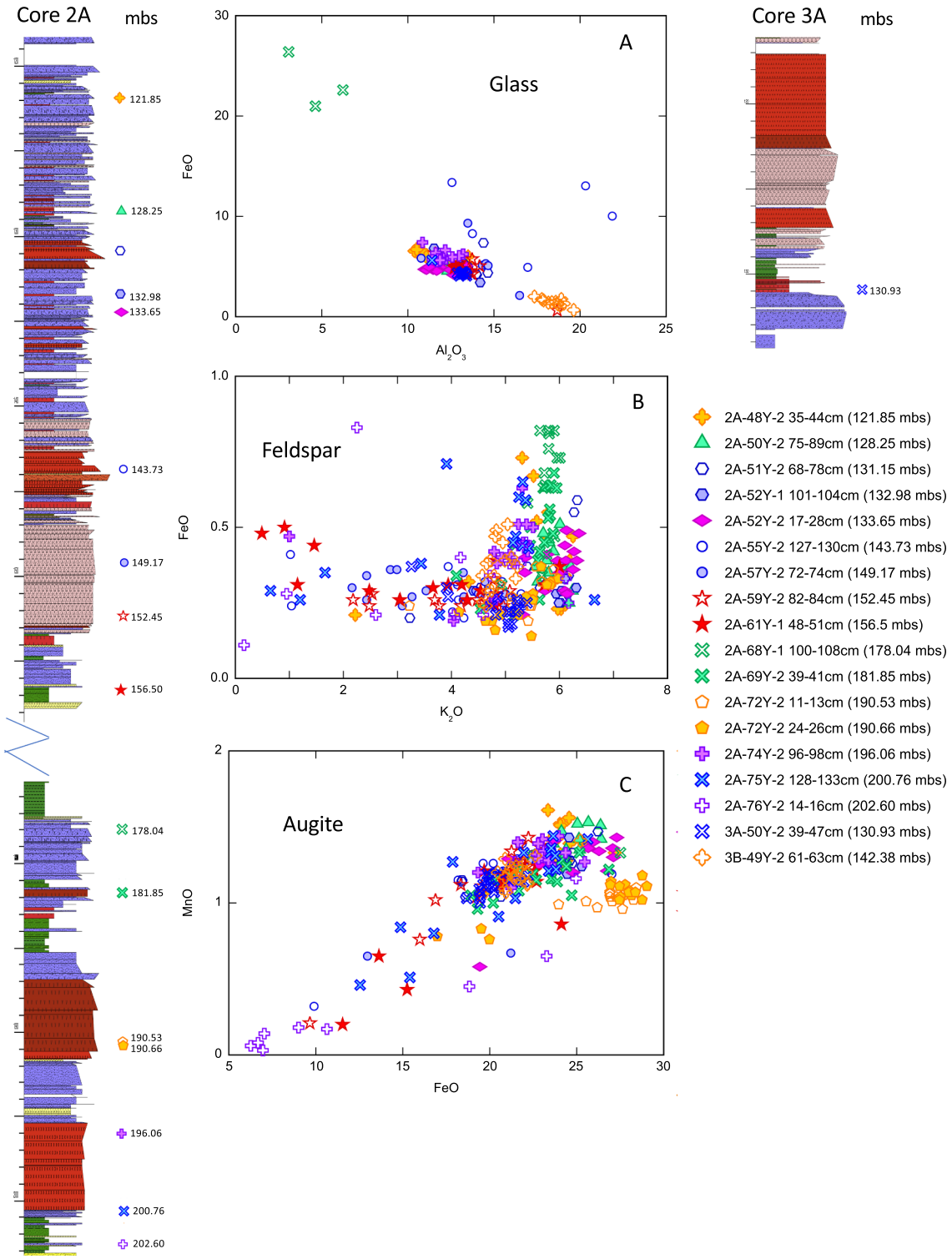

Fig. 13. Stratigraphy and compositional plots for the lower part of the Ngorongoro Formation, Cores 2A and 3A, below 120 mbs, additional plots. Same samples as Fig. 12. Key for colors (indicative of facies) in Fig. 3. A. Glass composition, FeO vs. Al_2O_3. Most samples plot together, with the trachyte from the base of Core 3B showing higher Al_2O_3 and the trachyandesite from Core 2A at 178.04 mbs with higher FeO. B. Feldspar compositions, FeO vs. K_2O. The trachyandesite at 178.04 mbs in Core 2A has elevated FeO in its anorthoclase. C. Augite compositions, MnO vs. FeO. The samples between 190.53 and 190.66 mbs in Core 2A are offset from the other samples in both MnO and FeO, and the 202.6 mbs sample (from near the base of the core) has much lower MnO and FeO.

"zone" approach to describe intervals of tuffs and volcaniclastic sediments sharing the mineralogical signature of one of the Olduvai Bed I marker tuffs (Tuffs IB, IC, ID) in the Junction Area in the vicinity of the *Zinjanthropus* site (Locality 45 of Hay, 1976). This approach was also taken further afield by Habermann et al. (2016). Thus, while a particular mineral assemblage and major element compositions of minerals cannot uniquely identify an individual unit, it can identify a short interval over which those compositions dominated.

The volcanic and volcaniclastic deposits of the older Ngorongoro Formation are similar in mineral assemblage and composition

throughout, largely dominated by anorthoclase feldspar, overlapping augite compositions, rare hornblende, and similar glass (rhyolite) compositions. Subtle mineralogical and geochemical distinctions help to distinguish the CFCT, Naabi, and Orkeri units from each other, though the volcanic units below are not systematically different from them. This suggests that all originated from the same source (Ngorongoro Volcano), which did not change much in composition during the deposition of the two major pulses of activity recorded in the OGCP cores. A few, individual units within the lower part of the Ngorongoro Formation do appear to have distinctive augite, anorthoclase, and glass compositions (described above), which could potentially help identify regional outcrop equivalents. In particular, the pyroclastic flow with its base at ~190.5 mbs in Core 2A has a tight population of distinctively FeO-rich augites, and the lowest volcanic unit in the cores (a coarse green crystal vitric tuff at ~202.6 mbs in Core 2A) has more MgO-rich augite compared to others analyzed in this project.

Future work will involve more in-depth analysis of the lower part of Core 3A (which was only coarsely sampled in the current study) to provide additional core-to-core correlations for the lower interval. As the $^{40}Ar/^{39}Ar$ dating of the core samples continues, this new age information will be incorporated into the tephrostratigraphic framework. For intervals of exceptional paleoanthropological interest (in Beds I and II), we can collect additional volcaniclastic sediment from the cores to help identify compositional "zones," even where the primary tuffs may be absent. Additional field sampling of tuffs and tuffaceous sandstones in the Upper Olduvai Beds (especially Masek and Ndutu, which are at present underrepresented in the comparative database) will further help with core-to-outcrop correlations. Comparison between the volcanic units in the lower part of the OGCP cores and tuffs exposed in the Naibadad Beds of Laetoli, which are rhyolitic and also thought to derive from Ngorongoro (McHenry, 2011), will help build a more regional tephrostratigraphic framework.

7. Conclusions

In this study we identified all of the major Upper Bed I tuffs in one or more of the three Cores 1A, 2A, 3A, using mineral assemblages and compositions, allowing for direct correlations between the paleoenvironmental records in the cores and outcrops in the Olduvai Basin. No specific correlations can be made between Bed II tuffs in the cores and outcrops based on mineral assemblage and composition alone, due in part to the poor preservation of these tuffs in lacustrine sediments. New tuff compositions, recognized in the cores but not yet known from outcrop, serve to correlate between the cores but will require follow-up field research to identify previously unrecognized minor tuffs within the Olduvai Bed II lacustrine strata. Below the Bed I basalts, the CFCT, Naabi, and Orkeri ignimbrites, known from outcrop exposures in the western gorge and along the First Fault to the southeast of Olduvai, are recognized based on mineral assemblage and composition in the upper part of the first of two major volcaniclastic fan complexes. Volcanic deposits below the Orkeri ignimbrite have no known outcrop analogs, but show that Ngorongoro was actively erupting rhyolites during at least two major intervals, culminating with the Naabi and CFCT eruptions. The tephrostratigraphic framework provided by these correlations helps relate the detailed paleoenvironmental record emerging from the OGCP cores directly to outcrops for critical parts of the Olduvai paleoanthropological record.

Supplementary data to this article can be found online at https://doi.org/10.1016/j.palaeo.2020.109630.

Declaration of competing interest

The authors avow that there are no conflicts of interest associated with this manuscript.

Acknowledgements

The authors would like to thank the Stone Age Institute for funding the Olduvai Gorge Coring Project (OGCP), with support from the Kaman Foundation, the Gordon and Ann Getty Foundation, the John Templeton Foundation, the Fred Maytag Foundation, Henry and Glenda Corning, and Kay and Frank Woods. Additional funding for the tephrostratigraphic work and core-to-outcrop correlations came from the National Science Foundation (BCS grant #1623884 to Njau and McHenry). We thank the Tanzanian Commission for Science and Technology (COSTECH), the Tanzanian Department of Antiquities, the Ministry of Natural Resources and Tourism, and the Ngorongoro Conservation Area Authority (NCAA) and the Commissioner of Mining for granting us permission to collect and export samples. Anders Noren, Kristina Brady, and the University of Minnesota LacCore facility were instrumental in the logging and sampling of the core, Christopher Vickery, Steven Greenwood, and Jordan Ludyan helped with sample preparation, Dr. John Fournelle greatly facilitated the EPMA analytical work, and Dr. Alan Deino provided the finer size fractions of his $^{40}Ar/^{39}Ar$ dating samples from the cores.

References

Ashley, G.M., Hay, R.L., 2002. Sedimentation patterns in a Plio-Pleistocene volcaniclastic rift-margin basin Olduvai Gorge, Tanzania. In: Ashley, G.M., Renaut, R.W. (Eds.), Sedimentation in Continental Rifts, SEPM Special Publication. 73. pp. 107–122.

Blumenschine, R.J., Stanistreet, I.G., Njau, J.K., Bamford, M.K., Masao, F.T., Albert, R.M., Stollhofen, H., Andrews, P., Prassack, K.A., McHenry, L.J., Fernández-Jalvo, Y., Camilli, E.L., Ebert, J.I., 2012. Environments and hominin activities across the FLK Peninsula during Zinjanthropus times (1.84 Ma), Olduvai Gorge, Tanzania. J. Hum. Evol. 63, 364–383.

Campisano, C.J., et al., 2017. The Hominin Sites and Paleolakes Drilling Project: high-resolution paleoclimate records from the East African Rift System and their implications for understanding the environmental context of hominin evolution. In: PaleoAnthropology. 2017. pp. 1–43. https://doi.org/10.4207/PA.2017.ART104.

Cohen, A., et al., 2016. The Hominin Sites and Paleolakes Drilling Project: inferring the environmental context of human evolution from eastern African rift lake deposits. Sci. Drill. 21, 1–16. https://doi.org/10.5194/sd-21-1-2016.

Deino, A.L., 2012. $^{40}Ar/^{39}Ar$ dating of Bed I, Olduvai Gorge, Tanzania, and the chronology of early Pleistocene climate change. J. Hum. Evol. 63, 251–273.

Greenwood, S.M., 2014. Mineralogy, Petrology, and Geochemistry of Pleistocene Volcanics at Embagai Caldera and Natron Basin, Tanzania: Potential Constraints on the Stratigraphy of Olduvai Gorge (M.S. Thesis). University of Wisconsin-Milwaukee.

Habermann, J.M., McHenry, L.J., Stollhofen, H., Tolosado-Delgado, R., Stanistreet, I.G., Deino, A.L., 2016. Discrimination, correlation, and provenance of Bed I tephrostratigraphic markers, Olduvai Gorge, Tanzania, based on multivariate analyses of phenocryst compositions. Sediment. Geol. 339, 115–133.

Hay, R.L., 1976. Geology of the Olduvai Gorge: A Study of Sedimentation in a Semiarid Basin. University of California Press, Berkeley (203 pp).

Hay, R.L., Kyser, T.K., 2001. Chemical sedimentology and paleoenvironmental history of Lake Olduvai, a Pliocene lake in northern Tanzania. Geol. Soc. Am. Bull. 113, 1505–1521.

Klein, R.G., 1999. The Human Career: Human Biological and Cultural Origins. University of Chicago Press, pp. 807.

Le Maitre, R., Bateman, P., Dudek, A., Keller, J., Lameyre, J., Le Bas, M., Sabine, P., Schmid, R., Sorensen, H., Streckeisen, A., Woolley, A., Zanettin, B., 1989. In: Le Maitre, R.W. (Ed.), A Classification of igneous rocks and glossary of terms: Recommendations of the International Union of Geological Sciences Subcommission on the Systematics of Igneous Rocks. Blackwell, Oxford (193 p).

Leakey, L.S.B., 1951. Olduvai Gorge. A Report on the Evolution of the Hand-axe Culture in Beds I–IV. Cambridge University Press, Cambridge (163 pp.).

Leakey, L.S.B., 1965. Olduvai Gorge 1951–61. A Preliminary Report on the Geology and Fauna 1. Cambridge University Press, Cambridge.

Leakey, L.S.B., 1966. Homo habilis, Homo erectus and Australopithecines. Nature 209, 1281–1297.

Leakey, M.D., 1971. Olduvai Gorge, Vol. 3. Excavations in Beds I and II, 1960–1963. Cambridge University Press, Cambridge (328 pp.).

Leakey, L.S.B., Tobias, P.V., Napier, J.R., 1964. A new species of the genus Homo from Olduvai Gorge. Nature 202, 5–7.

McHenry, L.J., 2004. Characterization and Correlation of Altered Plio-Pleistocene Tephra Using a "Multiple Technique" Approach: Case Study at Olduvai Gorge. Dissertation, Rutgers University, New Brunswick, Tanzania. Ph.D.

McHenry, L.J., 2005. Phenocryst composition as a tool for correlating fresh and altered tephra, Bed I, Olduvai Gorge, Tanzania. Stratigraphy 2, 101–115.

McHenry, L.J., 2009. Element mobility during zeolitic and argillic alteration of volcanic ash in a closed-basin lacustrine environment: Case study Olduvai Gorge, Tanzania. Chem. Geol. 265, 540–552.

McHenry, L.J., 2010. Element distribution between coexisting authigenic mineral phases in argillic and zeolitic altered tephra, Olduvai Gorge, Tanzania. Clay Clay Miner. 58

(5), 627–643.
McHenry, L.J., 2011. Geochemistry and mineralogy of Laetoli area tuffs: Lower Laetolil through Naibadad Beds. In: Harrison, T. (Ed.), Paleontology and Geology of Laetoli, Tanzania: Human Evolution in Context. Volume 1: Geology, Geochronology, Paleoecology and Paleoenvironment. Springer series Vertebrate Paleobiology and Paleoanthropology, pp. 121–141. https://doi.org/10.1007/978-90-481-9956-3_6.
McHenry, L.J., 2012. A revised stratigraphic framework for Olduvai Gorge Bed I based on tuff geochemistry. J. Hum. Evol. 63, 284–299.
McHenry, L.J., Stanistreet, I.G., 2018. Tephrochronology of Bed II, Olduvai Gorge, Tanzania, and placement of the Oldowan–Acheulean transition. J. Hum. Evol. 120, 7–18.
McHenry, L.J., Mollel, G.M., Swisher III, C.C., 2008. Compositional and textural correlations between Olduvai Gorge Bed I tephra and volcanic sources in the Ngorongoro volcanic highlands, Tanzania. Quat. Int. 178, 306–319.
McHenry, L.J., Stollhofen, H., Stanistreet, I.G., 2013. Use of single-grain geochemistry of cryptic tuffs and volcaniclastic sandstones improves the tephrostratigraphic framework of Olduvai Gorge, Tanzania. Quat. Res. 80, 235–247.
McHenry, L.J., Njau, J.K., de la Torre, I., Pante, M.C., 2016. Geochemical “fingerprints” for Olduvai Gorge Bed II tuffs and implications for the Oldowan–Acheulean transition. Quat. Res. 85, 147–158.
Mollel, G.E., Swisher III, C.C., 2012. The Ngorongoro Volcanic Highland and its relationships to volcanic deposits at Olduvai Gorge and East African Rift volcanism. J. Hum. Evol. 63, 274–299.
Stanistreet, I.G., McHenry, L.J., Stollhofen, H., de la Torre, I., 2018. Bed II Sequence Stratigraphic context of EF-HR and HWK EE archaeological sites, and the Oldowan/Acheulean succession at Olduvai Gorge, Tanzania. J. Hum. Evol. 120, 19–31.
Stanistreet, I.G., Stollhofen, H., Deino, A., McHenry, L.J., Toth, N., Schick, K., Njau, J.K., 2020. New Olduvai Basin stratigraphy and stratigraphic concepts revealed by OGCP cores into the Palaeolake Olduvai depocentre, Tanzania. Palaeogeography, Palaeoclimatology. Palaeoecology (This volume).
Stollhofen, H., Stanistreet, I.G., 2012. Plio-Pleistocene syn-sedimentary fault compartments underpin lake margin paleoenvironmental mosaic, Olduvai Gorge, Tanzania. In: Blumenschine, R.J., Masao, F.T., Stanistreet, I.G., Swisher, C.C. (Eds.), Five Decades after Zinjanthropus and Homo habilis: Landscape Paleoanthropology of Plio-Pleistocene Olduvai Gorge, Tanzania. J. Hum. Evol 63. pp. 309–327.
Stollhofen, H., Stanistreet, I.G., McHenry, L.J., Mollel, G.F., Blumenschine, R.J., Masao, F.T., 2008. Fingerprinting facies of the Tuff IF marker, catastrophe for early hominin palaeoecology, Olduvai Gorge, Tanzania. Palaeogeography, Palaeoclimatology, Palaeoecology 259, 382–409.